Biogeosciences, 20, 3073–3091, 2023
https://doi.org/10.5194/bg-20-3073-2023

Biogeosciences Open Access EGU

Absence of photophysiological response to iron addition in autumn phytoplankton in the Antarctic sea-ice zone

Asmita Singh[1,2], Susanne Fietz[1], Sandy J. Thomalla[2,8], Nicolas Sanchez[3], Murat V. Ardelan[3], Sébastien Moreau[4,5], Hanna M. Kauko[4], Agneta Fransson[4], Melissa Chierici[6], Saumik Samanta[1], Thato N. Mtshali[7], Alakendra N. Roychoudhury[1], and Thomas J. Ryan-Keogh[2]

[1]Department of Earth Sciences, University of Stellenbosch, Stellenbosch, South Africa
[2]Southern Ocean Carbon–Climate Observatory, CSIR, Cape Town, South Africa
[3]Department of Chemistry, Norwegian University of Science and Technology (NTNU), Trondheim, Norway
[4]Norwegian Polar Institute (NPI), Tromsø, Norway
[5]Centre for Ice, Cryosphere, Carbon and Climate, Department of Geosciences, UiT,
The Arctic University of Norway, Tromsø, Norway
[6]Institute of Marine Research, Fram Centre, Tromsø, Norway
[7]Oceans and Coasts, Department of Forestry, Fisheries, and the Environment, Cape Town, South Africa
[8]Marine and Antarctic Research for Innovation and Sustainability, University of Cape Town, Cape Town, South Africa

Correspondence: Thomas J. Ryan-Keogh (tryankeogh@csir.co.za)

Received: 17 December 2022 – Discussion started: 6 January 2023
Revised: 13 June 2023 – Accepted: 19 June 2023 – Published: 31 July 2023

Abstract. The high nutrient–low chlorophyll condition of the Southern Ocean is generally thought to be caused by the low bioavailability of micronutrients, particularly iron, which plays an integral role in phytoplankton photosynthesis. Nevertheless, the Southern Ocean experiences seasonal blooms that generally initiate in austral spring, peak in summer, and extend into autumn. This seasonal increase in primary productivity is typically linked to the seasonal characteristics of nutrient and light supply. To better understand the potential limitations on productivity in the Antarctic sea-ice zone (SIZ), the photophysiological response of phytoplankton to iron addition (2.0 nM $FeCl_3$) was investigated during autumn along the Antarctic coast off Dronning Maud Land. Five short-term (24 h) incubation experiments were conducted around Astrid Ridge (68° S) and along a 6° E transect, where an autumn bloom was identified in the region of the western SIZ. Surface iron concentrations ranged from 0.27 to 1.39 nM around Astrid Ridge, and 0.56 to 0.63 nM along the 6° E transect. Contrary to expectation, the photophysiological response of phytoplankton to iron addition, measured through the photosynthetic efficiency and the absorption cross-section for photosystem II, showed no significant responses. It is thus proposed that since the autumn phytoplankton in the SIZ exhibited a lack of an iron limitation at the time of sampling, the ambient iron concentrations may have been sufficient to fulfil the cellular requirements. This provides new insights into extended iron replete post-bloom conditions in the typically assumed iron deficient high nutrient–low chlorophyll Southern Ocean.

1 Introduction

The Southern Ocean plays an important role in the global drawdown of atmospheric carbon dioxide (CO_2) (Khatiwala et al., 2009; Takahashi et al., 2002, 2009), which is partially driven by the biological carbon pump through phytoplankton photosynthetic carbon uptake and export. Seasonal changes in the physical and chemical environment of the Southern Ocean are expected to modify the physiological (Deppeler and Davidson, 2017; Moore et al., 2013) and metabolic functions of phytoplankton and consequently the efficiency of the biological carbon pump (Boyd et al., 2007, 2010b). The primary factors that limit carbon fixation during phytoplankton photosynthesis in the Southern Ocean are the availability of light (Kirk, 1994; de Baar et al., 2005; Trim-

born et al., 2019) and several essential trace metals (Sunda, 1989; Lindsey and Scott, 2010; Wu et al., 2019; Browning et al., 2021; Hawco et al., 2022), particularly iron, which is a crucial co-factor for the functioning of photosynthetic proteins (Raven, 1990; Raven et al., 1999; Strzepek and Harrison, 2004). In addition, iron is needed for nitrate reductase, which is responsible for the reduction of nitrate to nitrite (Sunda, 1989; Milligan and Harrison, 2000; de Baar et al., 2005; Bazzani et al., 2023) and is also required for the synthesis of chlorophyll and the quenching of reactive oxygen species (Sunda and Huntsman, 1995; Diaz and Plummer, 2018). However, nitrate assimilation has a high iron (Milligan and Harrison, 2000; de Baar et al., 2005) and light (Lucas et al., 2007; Moore et al., 2007a, b) demand, which drives the high nutrient–low chlorophyll (HNLC) conditions characteristic of the Southern Ocean (Price et al., 1994; Milligan and Harrison, 2000; Lucas et al., 2007; Cochlan, 2008; Moore et al., 2013). Thus, independent of adequate amounts of macronutrient concentrations in surface waters, any limitation on the bioavailability of iron will potentially decrease the efficiency of these processes (Martin and Fitzwater, 1988; Moore et al., 2001; Lis et al., 2015; Yoon et al., 2018), affecting nutrient drawdown, photosynthesis, primary productivity, biomass accumulation, and community composition of surface phytoplankton in the Southern Ocean (de Baar et al., 1990; Geider and La Roche, 1994; Martin et al., 1991; Martin and Fitzwater, 1988; Biggs et al., 2022). Furthermore, any light limitation will exacerbate iron limitation due to the increase in iron demand under low light conditions (Strzepek et al., 2012, 2019; Boyd and Abraham, 2001), thus driving the frequent occurrence of iron-light co-limitation conditions in the Southern Ocean (Moore et al., 2013; Tagliabue et al., 2014; Ryan-Keogh et al., 2017; Trimborn et al., 2019).

Although the Southern Ocean is typically considered an "iron-limited" region, iron availability or limitation is not uniform and instead varies spatially and temporally. For instance, iron limitation is commonly associated with the pelagic waters of the Southern Ocean (Mitchell et al., 1991; Yoon et al., 2018), where summer dissolved iron (dFe) concentrations in surface waters are typically < 0.5 nM (Sedwick et al., 1999; Coale et al., 1999; Vink and Measures, 2001; Klunder et al., 2011); however, there are a number of regional exceptions. These include regions with an external iron source such as sea-ice and iceberg meltwaters (Lannuzel et al., 2008; Boyd and Ellwood, 2010; Smith et al., 2010; Boyd et al., 2012), hydrothermal vents (Klunder et al., 2011; Tagliabue et al., 2017; Ardyna et al., 2019), atmospheric dust (Martin and Fitzwater, 1988; Mahowald et al., 2005), continental margin input (Sedwick et al., 2008; Bowie et al., 2009), and island wake inputs (Pollard et al., 2007; Blain et al., 2008). Internal processes such as remineralization (Tagliabue et al., 2017), resupply through deep winter mixing (Tagliabue et al., 2014), cross-frontal mixing (Lutjeharms et al., 1985; Moore and Abbott, 2002), and storm-driven entrainment (Nicholson et al., 2019) can also provide iron to surface waters in support of phytoplankton production. Most of these sources vary seasonally; for example, in winter, iron is not generally considered limiting, as deep winter mixing entrains a seasonal resupply of iron (Tagliabue et al., 2014; Mtshali et al., 2019). Instead, due to the deep seasonal mixed layers, ice cover, and low sun angles, the availability of photosynthetically active radiation (PAR) can be suboptimal and considered the dominant factor limiting phytoplankton production in winter. In spring, phytoplankton blooms are initiated when there is sufficient light, driven by a shoaling of the mixed layer (Moore and Abbott, 2002; Thomalla et al., 2011) as well as retreating sea ice (Taylor et al., 2013) to support phytoplankton growth under nutrient replete conditions (Swart et al., 2015; de Baar et al., 1990; Hauck et al., 2015; Martin et al., 1990). Blooms typically subside when nutrients such as iron are depleted in late summer or early autumn (Tagliabue et al., 2014; Soppa et al., 2016; Hiscock et al., 2008). Grazing (Lancelot et al., 1993; Moreau et al., 2020; Kauko et al., 2021), bacteria, and viruses (Biggs et al., 2021) may also accelerate the blooms' demise. Iron supply mechanisms during a bloom, such as advection from continental margins (Sedwick et al., 2008; Bowie et al., 2009), remineralization (Tagliabue et al., 2017), and storm-driven entrainment (Swart et al., 2015; Nicholson et al., 2019) may sustain phytoplankton growth for an extended duration. However, it is not clear how applicable these resupply processes are to the Southern Ocean as a whole, and where and when each of these dominate.

In general, experiments that investigate the degree of iron limitation by testing the impact of iron addition on metabolic functions of phytoplankton have largely focussed on summer conditions in the open Southern Ocean. There is thus minimal information on the impact of iron addition in the sea-ice zone (SIZ) in autumn, when iron concentrations are expected to be low (Tagliabue et al., 2014; Lannuzel et al., 2016). One exception was a study by Van Oijen et al. (2004), where a single iron-light perturbation experiment examined carbon uptake in the marginal ice zone in autumn, but no conclusions were made on the driving factors of enhanced uptake. To address this knowledge gap, we undertook a number of iron addition experiments using active chlorophyll-*a* (Chl-*a*) fluorescence in the SIZ off Dronning Maud Land (DML) in autumn (March). Active Chl-*a* fluorescence is a key indicator of the photophysiological state of phytoplankton (Hughes et al., 2018; Brown et al., 2019; Schuback et al., 2021) and provides a powerful tool for evaluating the photophysiological response of phytoplankton to iron addition. This is done by measuring the photosynthetic efficiency, F_v/F_m, and the absorption cross-section of photosystem II, σ_{PSII} (Geider, 1993; Geider and La Roche, 1994; Kolber et al., 1988; 1994; Hughes et al., 2018). Any photophysiological response measured through active Chl-*a* fluorescence can, however, be due to both changes in cellular structure, i.e. a response seen on short timescales (milliseconds to femtoseconds), and changes in community composition, i.e. a

response seen on longer timescales (usually > 24 h). Since different phytoplankton groups tend to have different photophysiological signatures (Suggett et al., 2009), any measured response in photophysiology over longer time periods (> 24 h) is difficult to interpret, as it reflects both the cellular and community adjustments. This makes it difficult to resolve the physiological response of phytoplankton to iron addition in manipulation incubation experiments from community composition adjustments (Suggett et al., 2009).

Many iron addition incubation experiments previously conducted in the Southern Ocean (de Baar et al., 1990; Hinz et al., 2012; Ryan-Keogh et al., 2018; Viljoen et al., 2018; among others) were run for long time periods (> 96 h) and showed evidence of substantial changes in community composition, which are likely to influence the photophysiological signal and consequently the interpretation of iron limitation (Ryan-Keogh et al., 2013; Suggett et al., 2009). In this paper, we opted instead for short-term (24 h) incubation experiments to isolate changes in photophysiology, i.e. F_v/F_m and σ_{PSII}. This is in line with a study by Ryan-Keogh (2014), which tested whether 24 h was sufficient to allow a measurable photophysiological response in Southern Ocean phytoplankton, where low temperatures may control uptake kinetics. Ryan-Keogh (2014) compared the photophysiology between incubations running for 24 and 48 h in summer and found that the samples were iron-limited (i.e. the differences between unamended control and iron addition incubations were significant). However, no significant differences were observed in photophysiology following iron addition when comparing the incubations of 24 vs. 48 h, supporting the robustness of a representative response in photophysiology within 24 h. During this timeframe, the community composition is not expected to change, nor would we expect to see any adjustments in biomass or nutrient drawdown (Browning et al., 2014a; Ryan-Keogh et al., 2013, 2017). As such, this study reported here provides a unique investigation of the short-term photophysiological response of phytoplankton to iron addition in the SIZ in autumn, a season where iron limitation may be expected and a season and region that is under sampled. The experiments test the hypothesis that phytoplankton in the SIZ off DML experience iron limitation during post-bloom conditions in autumn.

2 Materials and methods

The focus of this study is on five short-term (24 h) incubation experiments performed in March during the Southern Ocean Ecosystem Cruise (cruise number DML2019702) between 28 February and 10 April 2019, on-board the Norwegian R/V *Kronprins Haakon* in the SIZ of the Kong Håkon VII Hav off the Dronning Maud Land coast, as well as the region surrounding the Astrid Ridge (Fig. 1). Ancillary data (i.e. Chl-*a* concentrations, macronutrient concentrations, and dFe concentrations) from surface water samples provide information on the regional conditions surrounding the five incubation experiments at the time of the cruise.

2.1 Underway and surface CTD seawater sampling and measurements

Underway seawater was obtained from the ship's clean seawater sampling system at ∼ 4 m depth between incubation stations. Samples were collected for determining Chl-*a* concentration, macronutrient concentrations (nitrate, phosphate, and silicate), and photophysiology (F_v/F_m and σ_{PSII}) (Kauko et al., 2020, 2021, 2022a, b; Chierici and Fransson, 2020; Singh et al., 2022). Additionally, surface seawater samples were collected using a Seabird CTD (conductivity–temperature–depth) rosette sampler and similarly analysed for Chl-*a*, macronutrients, and photophysiology in addition to phytoplankton community composition (Kauko et al., 2020, 2021, 2022a, b; Chierici and Fransson, 2020; Singh et al., 2022). Sample processing and analysis are further detailed in Sect. 2.4 for phytoplankton photosynthetic photophysiology and Sect. 2.5–2.10 for ancillary data. In addition, initial in situ conditions for the incubation experiments from CTD surface samples are detailed below in Sect. 2.3 (incubation set-up and sub-sampling).

2.2 Surface seawater sampling for incubation experiments

Seawater samples for experimental station Exp01 were collected at 20 m depth using a Watson-Marlow Varmeca (MG0723) peristaltic pump connected to PTFE tubing with a 10 mm inner diameter at a flow rate of 1.6 L min^{-1}. All sampling tubing (peristaltic and PTFE) and 1 L Polycarbonate bottles (Thermo Fisher Scientific Nalgene) were acid washed following GEOTRACES protocols (Cutter et al., 2017). Next, inside a custom-made HEPA air-filtered Class-100 trace metal clean "plastic bubble" that consisted of a clean, steady laminar flow hood (AirClean-600 PCR Workstation), the seawater was pumped into seven 1 L polycarbonate bottles, all this under strict trace metal clean conditions. For the other experiments (Exp02, Exp03, Exp04, and Exp05), a Teflon-lined, trace metal clean, external closure 8 L GoFlo bottle (General Oceanics) was deployed on an aramid rope (VGP Industries), using a dedicated winch and Teflon-coated messenger to ∼ 20–30 m depth for surface incubation seawater (i.e. for experimental stations Exp02, Exp03, Exp04, and Exp05). At each of the five experimental stations (see Fig. 2a and Table 1 for locations), seven 1 L polycarbonate bottles were filled unscreened (i.e. no large grazers were excluded from the bottles) with the incubation seawater to represent 1 times the initial sample (hereafter "initial"), 3 times the unamended control samples (hereafter "Control"), and 3 times the iron addition samples (hereafter "Fe"), which were spiked with 2.0 nM iron (III) chloride ($FeCl_3$ TraceCERT®; Sigma-Aldrich) prepared in 2 ‰ HCl

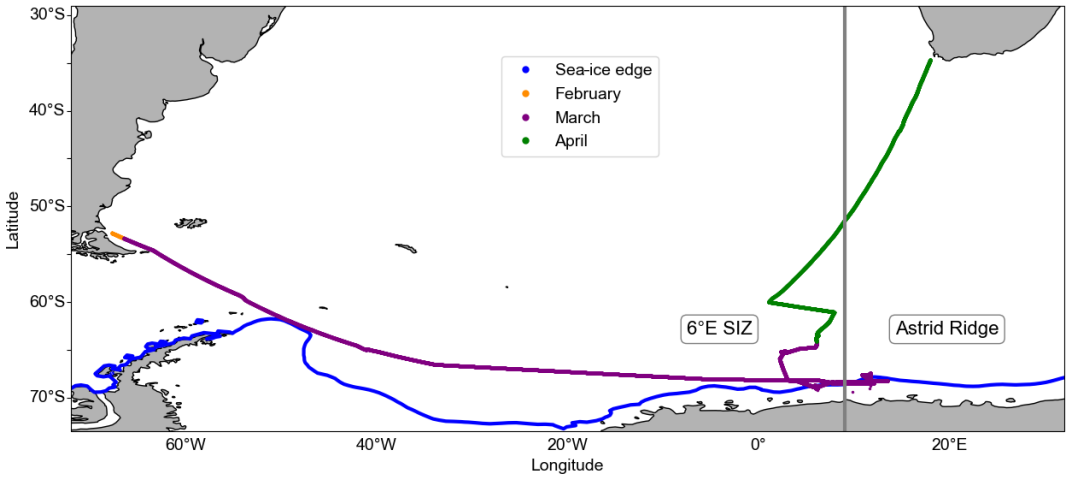

Figure 1. Map of the general study region depicting the cruise track of the DML2019702 cruise that began in Punta Arenas, Chile, on 28 February 2019; traversed the Atlantic Southern Ocean and the Dronning Maud Land sea-ice edge in March; and ended in Cape Town, South Africa, on 10 April 2019. The 6° E SIZ and Astrid Ridge regions are indicated, as well as the average sea-ice edge (concentration at 15 %) for March 2019 (Brodzik and Stewart, 2016).

(30 % Suprapur HCl; Merck), to reach a final concentration of 2.0 nM Fe. The bottle caps of the Control and Fe samples were sealed with Parafilm™, and the bottles were double-bagged in clear polyethylene bags (Ziploc™) to avoid sample contamination. All incubation bottle filling, spiking, and sub-sampling were performed under a clean, laminar flow hood (AirClean-600 PCR Workstation), inside a makeshift HEPA air-filtered Class-100 trace metal clean bubble on-board, under strict trace metal clean conditions.

2.3 Incubation set-up and sub-sampling

The incubation bottles were placed inside an on-deck incubator under natural sunlight, with flowing seawater, which fluctuated with the ocean temperature, passing through the incubator to mimic in situ seawater temperatures. The seawater temperature was measured at the ship's intake by a thermosalinograph. Light levels inside the polycarbonate bottles were approximated using a handheld 4π PAR sensor (Biospherical QSL 2100, Biospherical Instruments Inc.) with the Logger 2100 software. A green mesh was used to filter out a fraction of the PAR on Exp01, with the PAR approximated inside the incubator bottle being 37 % of sea surface PAR, whilst the remaining experiments had no filters on the incubators, and the average PAR inside the incubator bottle corresponded to 43 % PAR at the sea surface. After each 24 h period, the incubation bottles were removed from the incubator and sub-sampled under the clean, laminar flow hood (AirClean-600 PCR Workstation) inside the makeshift HEPA air-filtered Class-100 trace metal clean plastic bubble on-board as described above in Sect. 2.2. All incubation bottles were sub-sampled for photophysiological parameters using active Chl-*a* fluorescence measured through Fast Repetition Rate fluorometry (FRRf) (see Sect. 2.4), Chl-*a* concentration (see Sect. 2.5), and macronutrients (see Sect. 2.6). A complete list of sampling locations, initial parameters for the photophysiology, and ancillary data, as well as other relevant information (cumulative photon dose, MLD, euphotic depth, and sea surface layer temperatures), is provided in Table 1.

2.4 Phytoplankton photosynthetic photophysiology

Active Chl-*a* fluorescence was measured with a FastOcean™ FRRf incorporating a FastAct™ laboratory system (Chelsea Technology Group), operated with the single-turnover protocol set with a flash saturation sequence (100×1 µs flashlets with a 2 µs interval) and a relaxation sequence (25×1 µs with an interval of 84 µs). The power of the excitation LED ($\lambda_{450\,\mathrm{nm}}$) was adjusted between samples to saturate the observed transients following manufacturer specifications. All samples were dark acclimated for ~ 30 min under in situ temperatures prior to measurement of the photophysiological (fluorescence) parameters ($F_\mathrm{v}/F_\mathrm{m}$ and σ_PSII) (Roháček, 2002) and were each blank corrected using carefully prepared 0.2 µm filtrates (Cullen and Davis, 2003). The FRRf measurements were recorded with the FastPro8 software (v1.0.55), and post-processing analysis was done in Python 3.7, using the customized package Phytoplankton Photophysiology Utilities (Ryan-Keogh and Robinson, 2021). The fluorescence response data were fitted to the saturation phase of the biophysical model of Kolber et al. (1998), with a constant connectivity coefficient ρ of 0.3 (Suggett et al., 2001) to derive F_o, F_m, and $F_\mathrm{v}/F_\mathrm{m}$. The sample means and the standard deviation (SD) were calculated for $F_\mathrm{v}/F_\mathrm{m}$ and σ_PSII from each set of triplicate samples. Statistical *t* tests were performed to compare the mean $F_\mathrm{v}/F_\mathrm{m}$ and σ_PSII values between the Control and Fe samples. This was done using a Levene test to check for equal variance: if the data were of

Table 1. Sampling location information for the incubation stations and the associated CTD-Rosette water column station numbers from the cruise (CTD cast identifier) and mean ($n = 3$) initial parameters for the photophysiology (F_v/F_m and σ_{PSII}), as well as the associated ancillary data (i.e. Chl-*a* concentrations, macronutrient concentrations, and dFe concentrations). Cumulative photon dose and euphotic depth were calculated as defined in materials and methods. Mixed layer depth (MLD) was obtained from Kauko et al. (2021). The sea surface layer temperatures (SSLTs) averaged for depths 15 to 30 m were obtained from the CTD sensor. Dominant phytoplankton community composition was taken from a combination of microscopy and CHEMTAX data from Kauko et al. (2022a, b).

	Experiment				
	Exp01	Exp02	Exp03	Exp04	Exp05
CTD identifier	CTD53	CTD70	CTD83	CTD97	CTD105
Initiation date	12 Mar 2019	17 Mar 2019	19 Mar 2019	24 Mar 2019	26 Mar 2019
Initiation time (UTC)	08:18	08:33	19:34	23:26	09:12
Latitude (° S)	68.10	67.56	68.23	68.76	69.07
Longitude (° E)	6.00	11.75	13.51	6.09	6.03
Sunrise (UTC)	05:02	04:57	04:57	05:45	05:53
Sunset (UTC)	18:27	17:45	17:30	17:38	17:30
Cumulative photon dose (mol photons m^{-2} d^{-1})	124	156	160	93	92
MLD (m)	38	27	36	28	30
Euphotic depth (m)	31	50	n.d.	n.d.	53
Mean PAR in the mixed layer (µmol photons m^{-2} s^{-1})	16.65	109.86	n.d.	n.d.	134.08
SSLT (°C)	−0.33	−1.16	−1.76	−1.71	−1.86
F_v/F_m	0.20 ± 0.01	0.34 ± 0.02	0.35 ± 0.01	0.32 ± 0.03	0.28 ± 0.01
σ_{PSII} (nm^2)	3.99 ± 0.37	2.72 ± 0.08	2.45 ± 0.12	3.13 ± 0.54	2.92 ± 0.54
Chl-*a* (µg L^{-1})	0.73*	0.23*	0.02*	0.18*	0.14*
Nitrate (µM)	22.5*	26.2*	25.5*	25.8*	25.7*
Phosphate (µM)	1.67*	1.71*	1.69*	1.72*	1.75*
Silicate (µM)	43*	48*	48*	43*	44*
dFe (nM)	n.d.	0.86 ± 0.05	1.39 ± 0.14	0.56 ± 0.05	0.63 ± 0.13
dFe : nitrate (nmol : µmol)	n.d.	0.03	0.06	0.02	0.03
dFe : phosphate (nmol : µmol)	n.d.	0.05	0.82	0.33	0.36
Dominant phytoplankton community composition	High diatom abundance, flagellates, dinoflagellates	Pennate diatoms and centric diatoms	Pennate diatoms and centric diatoms	Flagellates	Flagellates

"n.d." indicates that no data were available, "±" precedes standard deviation ($n = 3$), and "*" denotes that a single measurement was performed.

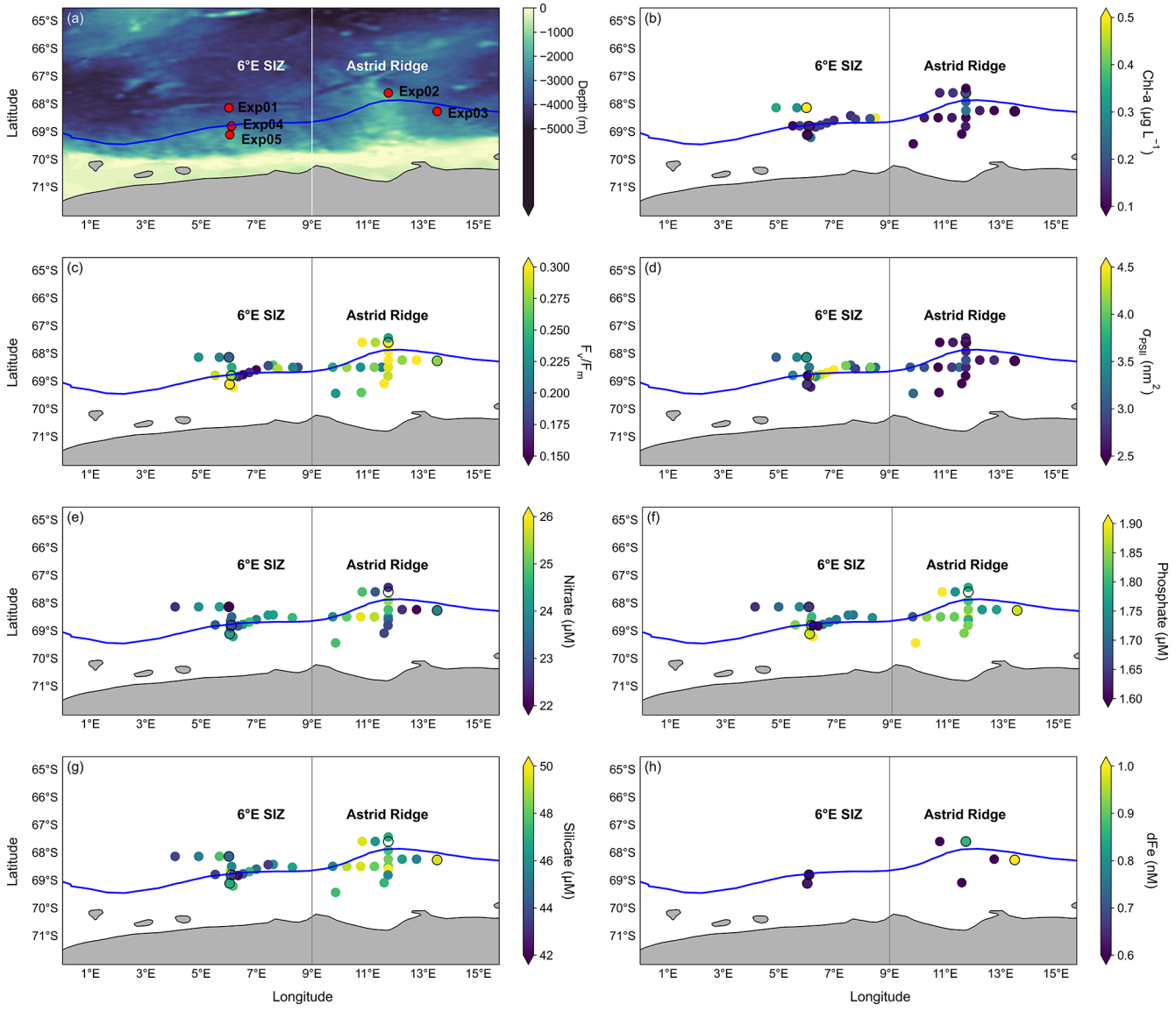

Figure 2. Initial conditions of the study region. Plots of **(a)** the overlaid bathymetry of the study region where the 6° E SIZ and Astrid Ridge regions are indicated, along with the sampling locations for the incubation experiments (during March), and the associated mean initial parameters for **(b)** Chl-*a* concentrations (µg L^{-1}), **(c)** F_v/F_m, **(d)** σ_{PSII} (nm^2), **(e)** nitrate (µM), **(f)** phosphate (µM), **(g)** silicate (µM), and **(h)** dFe concentration (nM). Discrete seawater samples from the underway system, surface CTD-Rosette and the GoFlo (from initial incubations), all sampled within the study region in March, are collectively presented in panels **(b)**–**(g)** along with the average sea-ice edge (concentration at 15 %) for March 2019 (blue line). Plot **(h)** shows the dFe concentrations which were sampled at all the GoFlo stations. All data for incubation stations are given in Table 1, and incubation stations are indicated by a black circle outline in panels **(b)**–**(h)**.

equal variance, a standard Student's *t* test was applied, while in the case of unequal variance, a Welch's *t* test was applied. Results of the *t* tests are reported as statistically significant at the 95 % confidence level (p value < 0.05).

2.5 Chlorophyll-*a* (Chl-*a*)

A volume of 500–1000 mL of seawater was filtered for Chl-*a* extraction onto GF/F filters (nominal pore size 0.7 µm; GE HealthCare) under low vacuum pressure (ca. −30 kPa). Chl-*a* was extracted with 100 % methanol at 4 °C in the dark for 24 h (Holm-Hansen and Riemann, 1978) and was subsequently measured on-board using a Turner 10AU Fluorometer (Turner Designs), which was calibrated prior to the cruise using a standard calibration curve from raw Chl-*a* (Sigma C6144). The uncertainty in Chl-*a* values was estimated as 5.5 % of the measured values during an earlier campaign utilizing the same method and instrument (Assmy et al., 2017).

2.6 Macronutrients

The seawater samples for macronutrient analysis (nitrate, phosphate, and silicate) were collected in 50 mL Falcon tubes for the incubation experiments and underway samples, whereas water column samples from the CTD-Rosette were collected in 20 mL vials. All samples were preserved with 250 µL of chloroform (saturated solution with 1 % ethanol for stabilization). The samples were kept cold (at 4 °C in a fridge) and in the dark until post-cruise analysis was performed using a spectrophotometric method following standard procedures (Grasshoff et al., 2009) at the Institute of Marine Research, Bergen, Norway, on a Skalar autoanalyser (Gundersen et al., 2022). The analyser was calibrated using reference seawater from Ocean Scientific International Ltd. The detection limits were 0.5 µM for nitrate, 0.06 µM for phosphate, and 0.7 µM for silicate. The uncertainty for nitrate and silicate was < 0.2 %, and it was < 1 % for phosphate (Gundersen et al., 2022).

2.7 Dissolved Fe (dFe)

Seawater samples for dFe measurements were collected from the clean GoFlo bottles (5 L General Oceanics) at seven stations in the study region (unfortunately, a dFe sample is not available for experimental station Exp01) into acid-washed 125 mL low-density polyethylene (LDPE, Nalgene, Thermo Scientific) sampling bottles. The LDPE bottles were acid cleaned according to the GEOTRACES protocols (Cutter et al., 2017) prior to the cruise. The dFe samples were filtered through sequential Sartorius capsule filters (0.45 and 0.2 µm pore size filtration) using acid-washed Tygon tubes inside the trace metal clean plastic bubble. During filtration, an additional HEPA air-filter cartridge (HEPA-CAP/HEPA VENT, 75 mm, Whatman) was connected to the pressure relief valve of the GoFlo bottles to ensure that the air in contact with the sample during the filtration was clean. All samples were acidified to pH < 2 with 600 µL of ~ 3 M double quartz distilled ultrapure HNO_3 (VWR, AnalaR NORMAPUR® analytical reagent), double-bagged, and stored at room temperature (> 2 years) until analysis at Stellenbosch University (TracEx, https://tracexsite.wordpress.com/ (last access: 25 July 2023), South Africa) as described in Samanta et al. (2021) using online pre-concentration methods. Although the samples were stored for more than 2 years before analysis, the dFe concentration is unlikely to be affected. The long-term analyses (2017–2021) of GEOTRACES and certified reference standards, which yielded consistent dFe concentrations, support this conclusion (Samanta et al., 2021). All samples were measured in duplicate. The detection limit of Fe was 0.08 nM, and the precision was 11 % (Samanta et al., 2021).

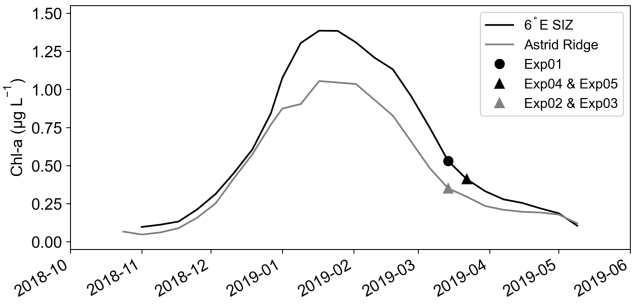

Figure 3. Satellite chlorophyll-*a* (Chl-*a*; µg L^{-1}) data from OC-CCI from 1 October 2018 to 1 June 2019. The 6° E SIZ (62–72° S; 0–9° E) and Astrid Ridge (62–72° S; 9–16° E) were created from spatial means, as indicated in the methods. The dates of the experimental set-ups are included for each region.

2.8 Satellite chlorophyll data

Ocean colour data (8 d, 4 km) were obtained from the ocean colour climate change initiation (OC-CCI) (Sathyendranath et al., 2019). In order to deduce missing data, satellite-derived Chl-*a* values were first re-gridded to a 4 km regular grid by averaging all data points within the new pixel dimensions. Gaps in the data were filled by applying a linear interpolation scheme as defined in Racault et al. (2014). The data were smoothed by applying a moving average filter of the previous and next time step (for more details on this method see Salgado-Hernanz et al., 2019). Two boxes were defined for the respective regions of this study and averaged to get the annual cycle of Chl-*a* concentration: 6° E SIZ (62–72° S; 0–9° E) and Astrid Ridge (62–72° S; 9–16° E) (Fig. 3).

2.9 PAR sensor data

The cumulative photon dose for each experiment (mol photons m^{-2} d^{-1}) was calculated as the cumulative sum of the PAR measured above the sea surface by a Biospherical/Licor Chelsea PAR sensor on the ship's mast, starting from the time of experimental commencement until experiment termination (i.e. summed over 24 h). Values were adjusted by ~ 43 % to account for shading within the incubator in accordance with the measured sea surface PAR inside the incubator.

2.10 Bathymetry data, stratification, the mixed layer depth (MLD), euphotic depth, and sea-ice concentration

The ETOPO1 bathymetry data for the study region were extracted from National Geophysical Data Center/NESDIS-/NOAA (U.S. Department of Commerce, 2011). The degree of stratification was obtained from the Brunt–Väisälä frequency (N^2; s^{-1}) (Millard et al., 1990), which was calculated using the seawater temperature, salinity, and potential density (σ) at each experimental station. The MLD for each exper-

imental station was obtained from Kauko et al. (2021), and the respective euphotic depth was determined as the depth at which PAR is 1 % of surface PAR, based on Kirk (1994). The sea-ice concentration was plotted at 15 % concentration for the sea-ice edge around Antarctica (Figs. 1 and 2) (Brodzik and Stewart, 2016).

3 Results

In previously published work from this cruise (Kauko et al., 2021), two distinct regions were identified in the DML SIZ. Both regions were visited in post-bloom conditions during the month of March (Kauko et al., 2021) but differed in the peak Chl-*a* concentrations, i.e. in the bloom amplitude (Fig. 3). The first region was in shallower bathymetry (2556 ± 724 m depth; 11–14° E, 67–69° S) around Astrid Ridge (Fig. 2a). Two short-term iron addition incubation experiments, Exp02 and Exp03, were conducted in this region, north and east of Astrid Ridge, respectively (Table 1; Fig. 2a). The second region in deeper bathymetry (3042 ± 1129 m depth, 5–7° E, 67–70° S) was located on a 6° E transect to the west of the Astrid Ridge in the open-ocean SIZ (6° E SIZ) (Fig. 2a), where the experimental station Exp01 was conducted. Despite being occupied in post-bloom conditions from a seasonal perspective (Fig. 3), Exp01 was, nonetheless, considered to represent autumn bloom conditions (Kauko et al., 2021; Moreau et al., 2023), albeit in decline, with a high Chl-*a* concentration ($0.73\,\mu g\,L^{-1}$, Table 1). Experimental stations Exp04 and Exp05 were sampled 2 weeks after Exp01, which was after the seasonal bloom (Chl-$a = 0.18\,\mu g\,L^{-1}$ and $0.14\,\mu g\,L^{-1}$, respectively) within the same 6° E SIZ region. We note that the starting time of each incubation was not synchronized (Table 1) and may lead to issues in interpreting photophysiological responses due to diurnal variation (Schuback et al., 2016). However, we found no distinct diurnal differences in both F_v/F_m and σ_{PSII} across the 6° E SIZ and Astrid Ridge regions (Fig. A3 in Appendix A), with both parameters showing very little variability between local sunrise and sunset.

Here, we first describe the general conditions in these two regions ($n = 34$) and then focus specifically on the five experimental stations. The Chl-*a* concentrations were lower around Astrid Ridge, ranging from 0.03 to $0.26\,\mu g\,L^{-1}$ (mean $0.12 \pm 0.07\,\mu g\,L^{-1}$; $n = 16$). Concentrations between 0.07 and $1.02\,\mu g\,L^{-1}$ (mean $0.25 \pm 0.24\,\mu g\,L^{-1}$; $n = 18$) were observed in the 6° E region of the SIZ (Fig. 2b; Table B1 in Appendix B). The mean values of F_v/F_m (Fig. 2c) were higher (p value < 0.05) at Astrid Ridge (0.28 ± 0.04) compared to the 6° E SIZ (0.24 ± 0.06). The 6° E SIZ showed a much larger range in F_v/F_m, with a minimum of 0.07 and a maximum of 0.34, whilst a narrower range in F_v/F_m, with a higher minimum in particular, was seen around Astrid Ridge (0.21 to 0.36). The σ_{PSII} (Fig. 2d) was typically higher in the 6° E SIZ region, ranging from 2.48 to $5.63\,nm^2$ (mean $3.41 \pm 0.71\,nm^2$) and lower around the Astrid Ridge, 1.93 to $3.56\,nm^2$ (mean $2.66 \pm 0.37\,nm^2$).

Surface nitrate concentrations showed some spatial variability, but the mean values were similar (p value > 0.05) for the 6° E SIZ (mean $23.8 \pm 0.8\,\mu M$) and Astrid Ridge (mean $24.0 \pm 1.2\,\mu M$) (Fig. 2e). Despite a similarity in the range of phosphate concentrations observed for both the regions from 1.57 to $1.96\,\mu M$ in the 6° E SIZ (mean $1.75 \pm 0.10\,\mu M$), and from 1.68 to $1.92\,\mu M$ at Astrid Ridge (mean $1.82 \pm 0.06\,\mu M$), the phosphate concentrations between the regions were significantly different (p value < 0.05) (Fig. 2f). Silicate concentrations showed a higher mean ($48 \pm 1\,\mu M$, p value < 0.05) and less variability around Astrid Ridge, with concentrations ranging from 46 to $52\,\mu M$, compared to a lower mean ($46 \pm 2\,\mu M$) and larger range (41 to $49\,\mu M$) observed in the 6° E SIZ (Fig. 2g). Despite the limited number of dFe measurements, a wide range of surface concentrations (Fig. 2h) were evident around Astrid Ridge, with concentrations as low as 0.27 nM and as high as 1.39 nM (mean 0.64 ± 0.49 nM). Mean dFe concentrations in the 6° E SIZ were slightly lower (0.59 ± 0.05 nM) compared to Astrid Ridge and varied over a narrow range between 0.56 and 0.63 nM. However, it is noted that only a fraction of the dFe is bioavailable to the phytoplankton, where this fraction can vary regionally and thus influence the variability in iron stress, which may not mirror the ambient concentrations (Lis et al., 2015). Furthermore, the mean PAR in the mixed layer for the 6° E SIZ was lower ($29.71\,\mu mol\,photons\,m^{-2}\,s^{-1}$) in comparison to the Astrid Ridge ($59.37\,\mu mol\,photons\,m^{-2}\,s^{-1}$).

In the following, we focus particularly on the upper ocean conditions at stations where incubation experiments were conducted (Table 1). Initial conditions in surface Chl-*a* ranged from high concentrations at the bloom station Exp01 ($0.73\,\mu g\,L^{-1}$) to concentrations as low as $0.02\,\mu g\,L^{-1}$ at Exp03 in the Astrid Ridge. Similar to the general oceanographic conditions, both nitrate and phosphate showed very little variability between experiments, whereas silicate concentrations were slightly lower for all three stations in the 6° E SIZ (43–44 µM) in comparison to the Astrid Ridge (48 µM). Unfortunately, the initial dFe concentration at the bloom station Exp01 is not available; however, dFe concentrations tended to be lower at the remaining stations (Exp04 and Exp05) in the 6° E SIZ (0.56–0.63 nM) compared to the Astrid Ridge (0.86–1.39 nM) (Table 1). The cumulative photon doses over 24 h (Table 1; Fig. A1) were substantially different, as Exp01, Exp02, and Exp03 (124–160 mol photons $m^{-2}\,d^{-1}$) had much higher doses compared to Exp04 and Exp05 (92–93 mol photons $m^{-2}\,d^{-1}$). The MLD at all experimental stations showed little variability (Kauko et al., 2020, 2021; Table 1; Fig. A2), ranging between 27 and 38 m (mean 31 ± 5 m). The degree of stratification, however, ranged substantially, being particularly stratified at the bloom station (Exp01), with a high degree of variability in the Brunt–Väisälä frequency (N^2) at

the MLD, and comparatively weakly stratified at Exp05, with very little variability in the profile of N^2 (Fig. A2). The euphotic depth ranged from 31 to 53 m at the three stations where CTD profiles were collected during daylight hours (Table 1). Since the euphotic depth was typically deeper than the MLD, these stations may unlikely be light-limited. However, mean PAR in the mixed layer had a broad range from 16.65 µmol photons m^{-2} s^{-1} (Exp01) to 134.08 µmol photons m^{-2} s^{-1} (Exp05) that likely reflects the degree of cloudiness (since time of day was similar), thus preventing us from making any definitive conclusions on light limitation. Although still in the negative, surface layer temperatures were warmer at the bloom station Exp01 (−0.33 °C) and cooler at the remaining stations (−1.16 to −1.86 °C) (Table 1).

Given the variability described above, it is anticipated that initial conditions of F_v/F_m and σ_{PSII} would vary between incubation stations (Table 1; Fig. 4). The F_v/F_m was lower in the 6° E SIZ (mean 0.27 ± 0.01) compared to Astrid Ridge (mean 0.35 ± 0.01) and much lower at the bloom station Exp01 (0.20 ± 0.01). The opposite was true for σ_{PSII}, with initial conditions being higher in the 6° E SIZ (mean 3.35 ± 0.28 nm^2) and the highest σ_{PSII} at Exp01 (3.99 ± 0.37 nm^2), with the lowest σ_{PSII} at the Astrid Ridge (mean 2.59 ± 0.05 nm^2). The differences in these initial conditions, i.e. seasonal timing and bloom amplitude, dFe surface concentrations, and F_v/F_m and σ_{PSII}, indicate that some variability in the photophysiological response to iron addition could be anticipated. Nonetheless, despite these initial differences in conditions, very little variability was observed in the photophysiological response to iron addition (Fe) relative to the Controls (Fig. 4; Table 2). A statistical t test between Fe and Control samples confirmed this, with no significant differences (p value > 0.05) in the photophysiology (F_v/F_m or σ_{PSII}) evident for any of the incubation experiments between treatments (Table 2). Similarly, no significant differences (p value > 0.05) were observed in either macronutrient or Chl-a concentrations (Table 2) between the Fe and Control incubations.

4 Discussion

The majority of Southern Ocean incubation studies have shown that phytoplankton are iron-limited (de Baar et al., 1990; Viljoen et al., 2018; Ryan-Keogh et al., 2017, 2018; Browning et al., 2014a, b). However, no studies, to our knowledge, have been conducted in the SIZ during autumn. Furthermore, the majority of these iron addition incubation studies were conducted as longer-term incubations (> 96 h). The complexity induced by longer-term nutrient addition incubations is exacerbated by artefacts that cause an isolated system to be devoid of natural factors. These natural factors include nutrient resupply and grazing, which differs between the initial and incubated samples, whilst retaining only a spe-

Table 2. Associated mean (± standard deviations) parameters of the Control and Fe samples measured post-incubation for F_v/F_m, σ_{PSII} (nm^2), and Chl-a concentrations (µg L^{-1}) and the macronutrients nitrate, phosphate, and silicate (µM). The letters "n.d." indicate that no data were available.

Experiment	F_v/F_m		σ_{PSII}		Chl-a		Nitrate		Phosphate		Silicate	
	Control	Fe	Control	Fe	Control	Fe	Control	Fe	Control	Fe	Control	Fe
Exp01	0.28 ± 0.01	0.29 ± 0.01	3.10 ± 0.26	3.15 ± 0.24	n.d.	0.97 ± 0.11	22.9 ± 0.2	23.0 ± 0.1	1.63 ± 0.02	1.68 ± 0.04	42 ± 0	42 ± 1
Exp02	0.22 ± 0.08	0.23 ± 0.05	2.56 ± 0.07	2.76 ± 0.34	0.19 ± 0.02	0.15 ± 0.02	26.4 ± 0.2	27.8 ± 0.6	1.66 ± 0.02	1.69 ± 0.01	48 ± 0	47 ± 1
Exp03	0.28 ± 0.06	0.29 ± 0.08	3.46 ± 0.90	3.07 ± 0.18	0.06 ± 0.02	0.05 ± 0.01	25.9 ± 0.1	25.7 ± 0.6	1.70 ± 0.00	1.69 ± 0.01	47 ± 0	47 ± 0
Exp04	0.33 ± 0.03	0.34 ± 0.03	3.51 ± 0.15	3.45 ± 0.16	0.18 ± 0.02	0.17 ± 0.01	26.0 ± 0.4	25.7 ± 0.6	1.74 ± 0.01	1.73 ± 0.01	44 ± 1	44 ± 0
Exp05	0.32 ± 0.04	0.32 ± 0.02	3.17 ± 0.22	3.02 ± 0.09	0.15 ± 0.00	0.13 ± 0.01	26.4 ± 0.4	26.1 ± 0.3	1.76 ± 0.01	1.74 ± 0.01	45 ± 0	46 ± 0

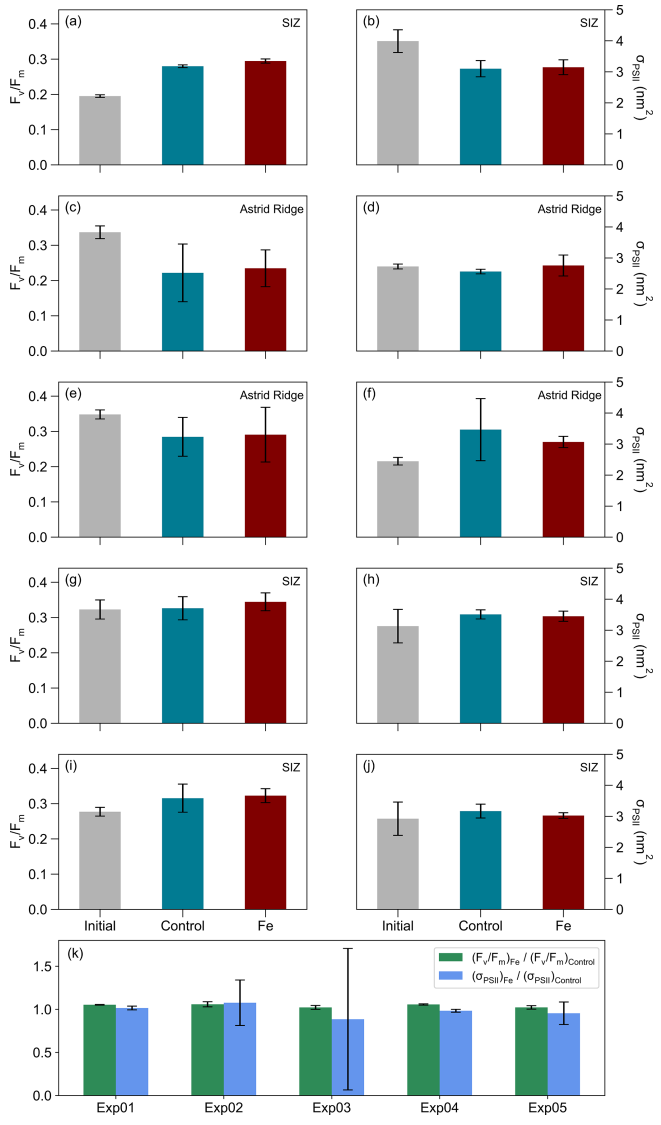

Figure 4. The mean ($n = 3$) F_v/F_m and mean σ_{PSII} (nm^2) from the initial, and the Control, and Fe treatments, where error bars indicate standard deviations. **(a, b)** Exp01, **(c, d)** Exp02, **(e, f)** Exp03, **(g, h)** Exp04, and **(i, j)** Exp05, while in panel **(k)** the ratio between the Fe and Control samples for F_v/F_m and σ_{PSII} are shown for each experiment, and error bars indicate standard deviations.

cific sampled section from the water column as representative of the entire system (Geider and La Roche, 1994). While short-term incubations, within 24 h, are also an isolated system devoid of these natural factors, the impacts of these factors are reduced in the shorter incubation timeframe and increased by the longer incubation timeframe. Thus, short-term incubation studies provide a sufficient period for eliciting a measurable photophysiological response (e.g. Ryan-Keogh et al., 2017), while at the same time minimizing the possibilities of artefacts in the incubation, as evidenced by the absence of any significant differences in phytoplankton biomass or nutrient concentrations between the Control samples after incubation and the initial samples before incubation. Indeed, other studies in the Southern Ocean have also reported significant changes in F_v/F_m within 24 h following iron addition (Boyd and Abraham, 2001; Hinz et al., 2012; Browning et al., 2014a, b; Ryan-Keogh et al., 2017), suggesting that it is possible to determine rapid (< 24 h) responses of photophysiology in iron-limited phytoplankton.

An annual time series of satellite-derived Chl-*a* averaged over the Astrid Ridge and 6° E SIZ region depicts the timing of the cruise relative to the seasonal cycle (Fig. 3) and clearly shows that both regional occupations were towards the end of the seasonal bloom. Therefore, it was anticipated that the region would be iron-limited and would respond favourably to iron addition. The study also covered a broad range of conditions when comparing the Astrid Ridge and 6° E SIZ regions (Fig. 2), i.e. shallower versus deeper bathymetry, lower versus higher biomass, lower versus higher dFe concentrations, lower versus higher F_v/F_m, and higher versus lower σ_{PSII}. Similarly, the average phytoplankton community composition between the two regions differed substantially (Kauko et al., 2022a, b), where pennate diatoms (72 %) and centric diatoms (56 %) dominated in the Astrid Ridge region (Exp02 and Exp03), while the 6° E SIZ region consisted mostly of flagellates (Exp04 and Exp05, 45 %), with the exception of Exp01 that together with flagellates had a high abundance of diatoms (74 %). Despite contrasting conditions in physics (density, stratification, cumulative photon dose, mean PAR in the mixed layer), chemistry (nitrate, silicate, and dFe) and biology (Chl-*a*, F_v/F_m, σ_{PSII}, and community composition), none of the five iron incubation experiments displayed any significant differences between the Fe and the Controls for photophysiology, or for any of the ancillary parameters (Table 1 and Figs. A1 and A2). As such, iron was not considered limiting to photosynthesis at any of the autumn stations in the DML SIZ. This unexpected finding implies that despite the timing of the cruise occupation relative to the seasonal bloom termination, iron was unlikely the primary driver of the bloom's termination (Kauko et al., 2021). Coincidently, Ryan-Keogh et al. (2023) proposed a greater probability of iron limitation in spring and summer in comparison to autumn and winter, which aligns with the results of our study. Furthermore, upon evaluating the initial dFe : nitrate (nmol : µmol) and dFe : phosphate (nmol : µmol) ratios (Table 1) for the experimental stations, it is worthy to note that the dFe : nitrate ratios appear to be higher than the reported values, for example, the wintertime assessment of dFe and nitrate distributions of Ellwood et al. (2008) in the south Tasman Sea of the Southern Ocean. Ellwood et al. (2008) reported a low range of dFe : nitrate ratios (0.005–0.018 nmol : µmol) further south from $\sim 52°$ S, which corresponded with other HNLC regions that reported iron-limiting conditions under low dFe : nitrate ratios (~ 0.01 nmol : µmol) (Ellwood et al., 2008 and references therein). Based on this evidence, the high dFe : nitrate ratios from our study (0.022–

0.055 nmol : µmol, Table 1) indicate very little probability for an iron limitation but rather limitations on light and other trace metals such as manganese instead (Wu et al., 2019; Browning et al., 2021; Hawco et al., 2022). The observed iron concentrations and these results suggest either an internal short-term or continuous supply of dFe that prevent the bloom from exhausting a finite dFe reservoir that would otherwise be expected so late in the growing season from a stratified water column. An example of the former mechanism could be a dFe supply from remineralization, in which high bacterial abundance could serve as a proxy (Boyd et al., 2010a; Tagliabue et al., 2017; Bressac et al., 2019) based on seasonal timing of the cruise occupation (i.e. post-bloom peak in autumn). This high bacterial abundance has been observed previously by Richert et al. (2019) during spring and summer in the Amundsen Sea, who suggested high bacterial abundance as a contributing factor to sustaining and promoting phytoplankton growth in autumn beyond the spring to summer bloom season. However, the bacterial abundance observed at both the Astrid Ridge (3.8×10^5 cells mL^{-1}) and in the southern section of the bloom region along the 6° E transect (3.9×10^5 cells mL^{-1}) was only slightly higher than at the bloom station Exp01 (2.6×10^5 cells mL^{-1}) (Kauko et al., 2021). These ranges were similar to the bacterial abundance previously observed in other Southern Ocean studies (Evans and Brussaard, 2012) and during different bloom phases (Fourquez et al., 2015; Christaki et al., 2021). Conversely, the external, continuous supply of dFe may be more viable, where anomalies in the easterly winds could drive sea ice southwards, favouring the upwelling of iron-rich, warmer deep water as suggested by Moreau et al. (2023). In addition, Kauko et al. (2021) utilized ∼ 20 years of satellite-derived ocean colour data to suggest that the high bloom magnitude in this region was enhanced by flow patterns in the Weddell Gyre and tidal current interactions with seafloor topography enhancing primary productivity by natural fertilization. And finally, considering factors that determine the bloom end, instead of a bottom-up or micronutrient limitation (e.g. a coastal manganese limitation; Wu et al., 2019; Browning et al., 2021), other factors such as high concentrations of krill swarms, which was observed by Kauko et al. (2021) around the 6° E transect, could suggest high levels of phytoplankton grazing, particularly in the Exp01 region (Moreau et al., 2023). Furthermore, bacteria, viral lysis, ice formation, wind mixing, and decreasing incident light may all be considered more important in curtailing the seasonal bloom in this particular region. Indeed, the ambient iron concentrations within the study region at the time of sampling may have been sufficient to fulfil the cellular requirements of the phytoplankton (Strzepek et al., 2011).

5 Conclusions

The results from this study show that although in theory it is expected that parts of the Southern Ocean are iron-limited during autumn, it is not necessarily true for the sea-ice zone region surrounding Astrid Ridge and along the 6° E transect. The observed in situ F_v/F_m and σ_{PSII} is suggestive of efficient photophysiology, since the iron addition did not lead to increased efficiency in phytoplankton photophysiology. The primary drivers of sustained iron supply to the region in support of phytoplankton growth late in the season are being potentially provided both from below (i.e. vertical supply from shallow bathymetry interactions with currents, as well as upwelling of iron-rich, warmer deep water) and from within (i.e. bacterial-driven remineralization). However, further examination of these sources and the type of iron being supplied is required to confirm the dominant resupply mechanism. It is recommended that future studies in this region help to bridge the knowledge gaps by studying the varying impacts of light in tandem with iron and other trace metals, which may instead be limiting during this time of the year, with an emphasis on short-term studies to understand the photophysiological response of phytoplankton in the absence of community induced responses.

Appendix A: Figures

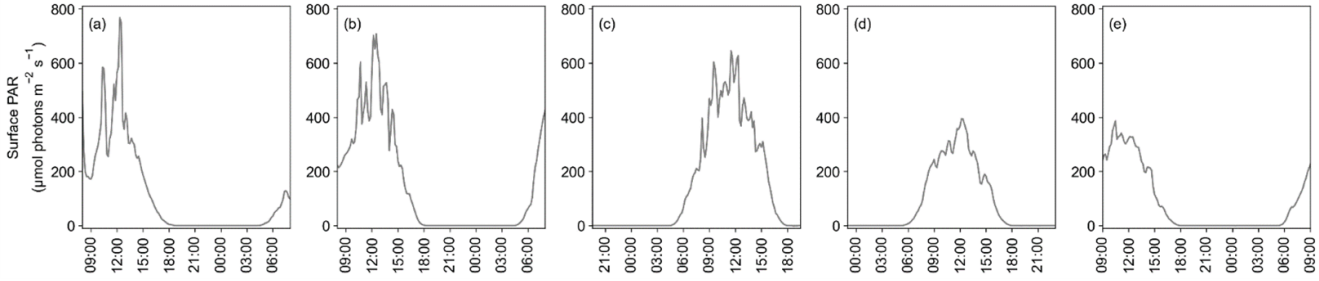

Figure A1. Surface PAR (µmol photons m^{-2} s^{-1}) at each experimental station **(a)** Exp01, **(b)** Exp02, **(c)** Exp03, **(d)** Exp04, and **(e)** Exp05. Data were plotted from the time of experimental set-up until the experiment was terminated 24 h later.

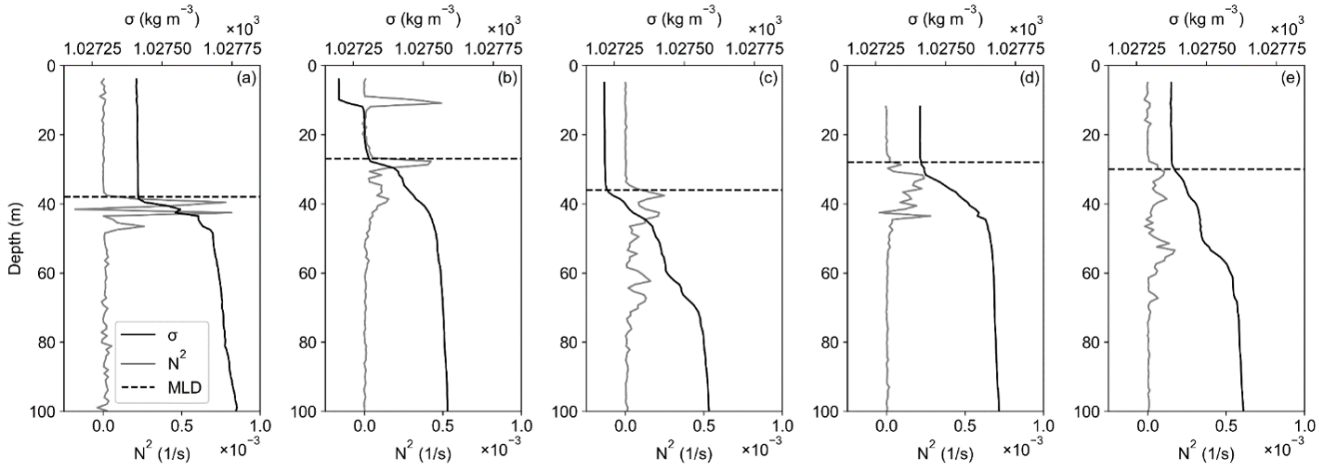

Figure A2. The depth profiles of density (σ; kg m^{-3}) and Brunt–Väisälä frequency (N^2) with the mixed layer depth (MLD; m) for experimental stations **(a)** Exp01, **(b)** Exp02, **(c)** Exp03, **(d)** Exp04, and **(e)** Exp05.

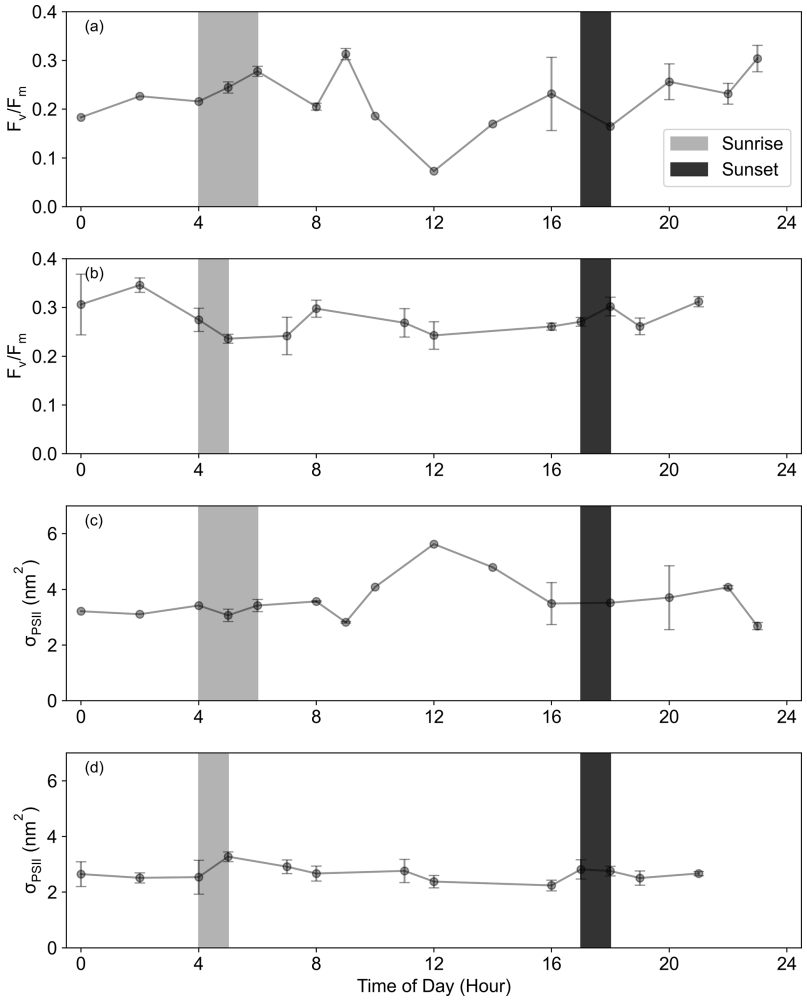

Figure A3. The diurnal cycle of **(a, b)** F_v/F_m for the **(a)** 6° E SIZ and **(b)** Astrid Ridge and of **(c, d)** σ_{PSII} for the **(c)** 6° E SIZ and **(d)** Astrid Ridge, where the range of local sunrise and sunset times are indicated. Data were averaged together using the hour of the day, where error bars indicate standard deviation.

Appendix B: Table

Table B1. Associated numbers (n), minimum, maximum, and mean ($\pm$ standard deviations) parameters for the 6° E SIZ and the Astrid Ridge for Chl-a concentrations ($\mu g\,L^{-1}$), F_v/F_m, σ_{PSII} (nm^2), macronutrients nitrate, phosphate, and silicate (µM) and the dFe concentrations (nM).

		Chl-a	F_v/F_m	σ_{PSII}	Nitrate	Phosphate	Silicate	dFe
6° E SIZ	min	0.07	0.07	2.48	21.8	1.57	41	0.57
	max	1.02	0.34	5.63	24.8	1.96	49	0.63
	mean $\pm$ SD	0.25 ± 0.24	0.24 ± 0.06	3.41 ± 0.71	23.8 ± 0.8	1.75 ± 0.10	45 ± 2	0.59 ± 0.05
	n	18	33	33	21	21	21	2
Astrid Ridge	min	0.03	0.21	1.93	21.8	1.68	46	0.27
	max	0.26	0.36	3.56	25.9	1.92	52	1.39
	mean $\pm$ SD	0.12 ± 0.07	0.28 ± 0.04	2.66 ± 0.37	24.0 ± 1.2	1.82 ± 0.06	48 ± 2	0.64 ± 0.49
	n	16	55	55	17	17	17	5

Data availability. All datasets on the underway samples (chlorophyll-*a*, photophysiology (F_v/F_m and σ_{PSII}) and nutrients (nitrate, phosphate, and silicate)), as well as the incubation data which appear in this paper, are available on Zenodo https://doi.org/10.5281/Zenodo.6322942 (Singh et al., 2022); the CTD-Rosette surface photophysiology data and the surface iron data from the GoFlo can also be found at this link. Full datasets for the other CTD-Rosette water column data are available at the Norwegian Polar Data Centre; Norwegian Polar Institute, https://doi.org/10.21334/npolar.2021.5e510f85 (chlorophyll-*a* and mixed layer depth; Kauko et al., 2020); and Norwegian Marine Data Centre, https://doi.org/10.21335/NMDC-1503664923 (nutrients; Chierici and Fransson, 2020).

Author contributions. TJRK and SJT conceptualized the study. AS and TJRK collected the data and performed the data analysis. MVA, NS, and AS conducted the trace metal clean water collection and sampling. SM planned the general biological sampling of the cruise. SM and HMK assisted in collecting and analysing the chlorophyll-*a* data and all the CTD-Rosette samples. SS and AS analysed the dissolved iron samples, SS performed the data analysis, and ANR guided the analysis of the dissolved iron samples. AF was the PI for the SANOCEAN and SOPHY-CO_2 project and was involved in cruise planning of the water column sampling onboard the cruise. MC was responsible for water column collection and analyses of all the nutrient samples obtained from the underway, water column, and incubation experiments. TNM supported preparations for the iron addition incubations. AS and TJRK produced the figures. AS wrote the initial paper. TJRK, SF, SJT, and AS contributed to the study design, interpretation of the results, and writing of the paper. All authors contributed to commenting on the paper.

Competing interests. The contact author has declared that none of the authors has any competing interests.

Disclaimer. Publisher's note: Copernicus Publications remains neutral with regard to jurisdictional claims in published maps and institutional affiliations.

Special issue statement. This article is part of the special issue "The Weddell Sea and the ocean off Dronning Maud Land: unique oceanographic conditions shape circumpolar and global processes – a multi-disciplinary study (OS/BG/TC inter-journal SI)". It is not associated with a conference.

Acknowledgements. We would like to acknowledge the support and assistance of the captain and crew of the R/V *Kronprins Haakon*, along with all the participants on the DML2019702 Ecosystem research cruise. Thank you to Agneta Fransson (NPI) and Sandy Thomalla (CSIR) as the PIs of the SANOCEAN project SOPHY-CO_2.

Financial support. The research expedition, Dronning Maud Land Ecosystem Cruise 2019, and the research conducted on the R/V *Kronprins Haakon* were part of a South African–Norwegian collaboration (SANOCEAN SOPHY-CO_2), funded by the National Research Foundation (NRF), South Africa (grant UID 118715); the Research Council of Norway (RCN; project number 288370); and the Norwegian Polar Institute (NPI), as well as additional financial support from the Norwegian Ministry of Foreign Affairs. Asmita Singh, Sandy J. Thomalla, and Thomas J. Ryan-Keogh were supported through the CSIR's Southern Ocean Carbon–Climate Observatory (SOCCO) Programme (http://socco.org.za/, last access: 25 July 2023) funded by the Department of Science and Innovation (DST/CON 0182/2017) and the CSIR's Parliamentary Grant. Funding was received from a number of grants from the National Research Foundation, South Africa: grant numbers 110731 (Susanne Fietz), 91313 (Susanne Fietz), 118751 (Sandy J. Thomalla), and 110729 (Sandy J. Thomalla).

Review statement. This paper was edited by Mario Hoppema and reviewed by three anonymous referees.

References

Ardyna, M., Lacour, L., Sergi, S., D'Ovidio, F., Sallée, J. B., Rembauville, M., Blain, S., Tagliabue, A., Schlitzer, R., Jeandel, C., and Arrigo, K.R.: Hydrothermal vents trigger massive phytoplankton blooms in the Southern Ocean, Nat. Commun., 10, 2451, https://doi.org/10.1038/s41467-019-09973-6, 2019.

Assmy, P., Fernández-Méndez, M., Duarte, P., Meyer, A., Randelhoff, A., Mundy, C. J., Olsen, L. M., Kauko, H. M., Bailey, A., Chierici, M., and Cohen, L.: Leads in Arctic pack ice enable early phytoplankton blooms below snow-covered sea ice, Sci. Rep., 7, 40850, https://doi.org/10.1038/srep40850, 2017.

Bazzani, E., Lauritano, C., and Saggiomo, M.: Southern Ocean Iron Limitation of Primary Production between Past Knowledge and Future Projections, Journal of Marine Science and Engineering, 11, 272, https://doi.org/10.3390/jmse11020272, 2023.

Biggs, T. E., Huisman, J., and Brussaard, C. P.: Viral lysis modifies seasonal phytoplankton dynamics and carbon flow in the Southern Ocean, ISME J., 15, 3615–3622, https://doi.org/10.1038/s41396-021-01033-6, 2021.

Biggs, T. E. G., Rozema, P. D., Evans, C., Timmermans, K. R., Meredith, M. P., Pond, D. W., and Brussaard, C. P. D.: Control of Antarctic phytoplankton community composition and standing stock by light availability, Polar Biol., 45, 1635–1653, https://doi.org/10.1007/s00300-022-03094-5, 2022.

Blain, S., Sarthou, G., and Laan, P.: Distribution of dissolved iron during the natural iron-fertilization experiment KEOPS (Kerguelen Plateau, Southern Ocean), Deep-Sea Res. Pt. II, 55, 594–605, https://doi.org/10.1016/j.dsr2.2007.12.028, 2008.

Bowie, A. R., Lannuzel, D., Remenyi, T. A., Wagener, T., Lam, P. J., Boyd, P. W., Guieu, C., Townsend, A. T., and Trull, T. W.: Biogeochemical iron budgets of the Southern Ocean south of Australia: Decoupling of iron and nutrient cycles in the subantarctic zone by the summertime supply, Global Biogeochem. Cy., 23, GB4034, https://doi.org/10.1029/2009GB003500, 2009.

Boyd, P. W. and Abraham, E. R.: Iron-mediated changes in phytoplankton photosynthetic competence during SOIREE, Deep-Sea Res. Pt. II, 48, 2529–2550, https://doi.org/10.1016/S0967-0645(01)00007-8, 2001.

Boyd, P. W. and Ellwood, M. J.: The biogeochemical cycle of iron in the ocean, Nat. Geosci., 3, 675–682, https://doi.org/10.1038/ngeo964, 2010.

Boyd, P. W., Jickells, T., Law, C. S., Blain, S., Boyle, E. A., Buesseler, K. O., Coale, K. H., Cullen, J. J., de Baar, H. J. W., Follows, M., Harvey, M., Lancelot, C., Levasseur, M., Owens, N. P. J., Pollard, R., Rivkin, R. B., Sarmiento, J., Schoemann, V., Smetacek, V., Takeda, S., Tsuda, A., Turner, S., and Watson, A. J.: Mesoscale Iron Enrichment Experiments 1993-2005: Synthesis and Future Directions, Science, 315, 612–617, https://doi.org/10.1126/science.1131669, 2007.

Boyd, P. W., Ibisanmi, E., Sander, S. G., Hunter, K. A., and Jackson, G. A.: Remineralization of upper ocean particles: Implications for iron biogeochemistry, Limnol. Oceanogr., 55, 1271–1288, https://doi.org/10.4319/lo.2010.55.3.1271, 2010a.

Boyd, P. W., Strzepek, R., Fu, F., and Hutchins, D. A.: Environmental control of open-ocean phytoplankton groups: Now and in the future, Limnol. Oceanogr. 55, 1353–1376, https://doi.org/10.4319/lo.2010.55.3.1353, 2010b.

Boyd, P. W., Arrigo, K. R., Strzepek, R., and Van Dijken, G. L.: Mapping phytoplankton iron utilization: Insights into Southern Ocean supply mechanisms, J. Geophys. Res.-Ocean, 117, C06009, https://doi.org/10.1029/2011JC007726, 2012.

Bressac, M., Guieu, C., Ellwood, M. J., Tagliabue, A., Wagener, T., Laurenceau-Cornec, E. C., Whitby, H., Sarthou, G., and Boyd, P. W.: Resupply of mesopelagic dissolved iron controlled by particulate iron composition, Nat. Geosci., 12, 995–1000, https://doi.org/10.1038/s41561-019-0476-6, 2019.

Brodzik, M. J. and Stewart, J. S.: Near-Real-Time SSM/I-SSMIS EASE-Grid Daily Global Ice Concentration and Snow Extent, Version 5, Distributed by NASA National Snow and Ice Data Center Distributed Active Archive Center [data set], https://doi.org/10.5067/3KB2JPLFPK3R, 2016.

Brown, M., Penta, W. B., Jones, B., and Behrenfeld, M.: The ratio of single-turnover to multiple-turnover fluorescence varies predictably with growth rate and cellular chlorophyll in the green alga Dunaliella tertiolecta, Photosynth. Res., 140, 65–76, https://doi.org/10.1007/s11120-018-00612-7, 2019.

Browning, T. J., Bouman, H. A., Moore, C. M., Schlosser, C., Tarran, G. A., Woodward, E. M. S., and Henderson, G. M.: Nutrient regimes control phytoplankton ecophysiology in the South Atlantic, Biogeosciences, 11, 463–479, https://doi.org/10.5194/bg-11-463-2014, 2014a.

Browning, T. J., Bouman, H. A., Henderson, G. M., Mather, T. A., Pyle, D. M., Schlosser, C., Woodward, E. M. S., and Moore, C. M.: Strong responses of Southern Ocean phytoplankton communities to volcanic ash, Geophys. Res. Lett., 41, 2851–2857, https://doi.org/10.1002/2014GL059364, 2014b.

Browning, T. J., Achterberg, E. P., Engel, A., and Mawji, E.: Manganese co-limitation of phytoplankton growth and major nutrient drawdown in the Southern Ocean, Nat. Commun., 12, 884, https://doi.org/10.1038/s41467-021-21122-6, 2021.

Chierici, M. and Fransson, A.: Nutrient data (nitrate, phosphate and silicate) in the eastern Weddell gyre, Kong Haakon VII Hav, and the coast of Dronning Maud Land in the Atlantic sector of the Southern Ocean in March 2019, Norwegian Marine Data Centre [data set], https://doi.org/10.21335/NMDC-1503664923, 2020.

Christaki, U., Gueneugues, A., Liu, Y., Blain, S., Catala, P., Colombet, J., Debeljak, P., Jardillier, L., Irion, S., Planchon, F., and Sassenhagen, I.: Seasonal microbial food web dynamics in contrasting Southern Ocean productivity regimes, Limnol. Oceanogr., 66, 108–122, https://doi.org/10.1002/lno.11591, 2021.

Coale, K. H., Worsfold, P., and de Baar, H.: Iron age in oceanography, EOS T. Am. Geophys. Un., 80, 377–382, https://doi.org/10.1029/EO080i034p00377-02, 1999.

Cochlan, W. P.: Nitrogen uptake in the Southern Ocean, in: Nitrogen in the Marine Environment, edited by: Capone, D. G., Bronk, D. A., Mulholland, M. R., and E. J. Carpenter, 2nd Edn., Academic Press, Elsevier, https://doi.org/10.1016/B978-0-12-372522-6.00012-8, 2008

Cullen, J. J. and Davis, R. F.: The Blank can Make a Big Difference in Oceanographic Measurements, Limnol. Oceanogr. Bull., 12, 29–35, https://doi.org/10.1002/lob.200413229, 2003.

Cutter, G., Casciotti, K., Croot, P., Geibert, W., Heimbürger, L.-E., Lohan, M., Van De Flierdt, T., and Planquette, H.: Sampling and Sample-handling Protocols for GEOTRACES Cruises, Version 3, August 2017, Toulouse, France, GEOTRACES International Project Office, https://doi.org/10.25607/OBP-2, 2017.

de Baar, H. J., Buma, A. G., Nolting, R., Cadee, G., Jacques, G., and Treguer, P.: On iron limitation of the Southern Ocean: experimental observations in the Weddell and Scotia Seas, Mar. Ecol.-Prog. Ser., 65, 105–122, https://doi.org/10.3354/meps065105, 1990.

de Baar, H. J. W., Boyd, P. W., Coale, K. H., Landry, M. R., Tsuda, A., Assmy, P., Bakker, D. C. E., Bozec, Y., Barber, R. T., Brzezinski, M. A., Buesseler, K. O., Boyé, M., Croot, P. L., Gervais, F., Gorbunov, M. Y., Harrison, P. J., Hiscock, W. T., Laan, P., Lancelot, C., Law, C. S., Levasseur, M., Marchetti, A., Millero, F. J., Nishioka, J., Nojiri, Y., van Oijen, T., Riebesell, U., Rijkenberg, M. J. A., Saito, H., Takeda, S., Timmermans, K. R., Veldhuis, M. J. W., Waite, A. M., and Wong, C. S.: Synthesis of iron fertilization experiments: From the iron age in the age of enlightenment, J. Geophys. Res.-Ocean, 110, 1–24, https://doi.org/10.1029/2004JC002601, 2005.

Deppeler, S. L. and Davidson, A. T.: Southern Ocean Phytoplankton in a Changing Climate, Front. Mar. Sci. 4, 40, https://doi.org/10.3389/fmars.2017.00040, 2017.

Diaz, J. M. and Plummer, S.: Production of extracellular reactive oxygen species by phytoplankton: past and future directions, J Plankton Res., 40, 655–666, https://doi.org/10.1093/plankt/fby039, 2018.

Ellwood, M. J., Boyd, P. W., and Sutton, P.: Winter-time dissolved iron and nutrient distributions in the Subantarctic Zone from 40–52S; 155–160E, Geophys. Res. Lett., 35, L11604, https://doi.org/10.1029/2008GL033699, 2008.

Evans, C. and Brussaard, C. P. D.: Regional variation in lytic and lysogenic viral infection in the Southern Ocean and its contribution to biogeochemical cycling, Appl. Environ. Microb., 78, 6741–6748, https://doi.org/10.1128/AEM.01388-12, 2012.

Fourquez, M., Obernosterer, I., Davies, D. M., Trull, T. W., and Blain, S.: Microbial iron uptake in the naturally fertilized waters in the vicinity of the Kerguelen Islands:

phytoplankton–bacteria interactions, Biogeosciences, 12, 1893–1906, https://doi.org/10.5194/bg-12-1893-2015, 2015.

Geider, R. J.: Quantitative phytoplankton physiology: implications for primary production and phytoplankton growth, ICES Mar. Sci. Symp., 197, 52–62, 1993.

Geider, R. J. and La Roche, J.: The role of iron in phytoplankton photosynthesis, and the potential for iron-limitation of primary productivity in the sea, Photosynth. Res., 39, 275–301, https://doi.org/10.1007/BF00014588, 1994.

Grasshoff, K., Kremling, K., and Ehrhardt, M.: Methods of Seawater Analysis, 3rd Edn., Hoboken, NJ, Wiley-VCH, ISBN 978-3-527-61399-1, 2009.

Gundersen, K., Møgster, J. S., Lien, V. S., Ershova, E., Lunde, L. F., Arnesen, H., and Olsen, A. K.: Thirty Years of Nutrient Biogeochemistry in the Barents Sea and the adjoining Arctic Ocean, 1990–2019, Sci. Data, 9, 649, https://doi.org/10.1038/s41597-022-01781-w, 2022.

Hauck, J., Völker, C., Wolf-Gladrow, D. A., Laufkötter, C., Vogt, M., Aumont, O., Bopp, L., Buitenhuis, E. T., Doney, S. C., Dunne, J., and Gruber, N.: On the Southern Ocean CO_2 uptake and the role of the biological carbon pump in the 21st century, Global Biogeochem. Cy., 29, 1451–1470, https://doi.org/10.1002/2015GB005140, 2015.

Hawco, N. J., Tagliabue, A., and Twining, B. S.: Manganese Limitation of Phytoplankton Physiology and Productivity in the Southern Ocean, Global Biogeochem. Cy., 36, e2022GB007382, https://doi.org/10.1029/2022GB007382, 2022.

Hinz, D. J., Nielsdóttir, M. C., Korb, R. E., Whitehouse, M. J., Poulton, A. J., Moore, C. M., Achterberg, E. P., and Bibby, T. S.: Responses of microplankton community structure to iron addition in the Scotia Sea, Deep-Res. Pt. II, 59–60, 36–46, https://doi.org/10.1016/j.dsr2.2011.08.006, 2012.

Hiscock, M. R., Lance, V. P., Apprill, A. M., Bidigare, R. R., Johnson, Z. I., Mitchell, B. G., Smith, W. O., and Barber, R. T.: Photosynthetic maximum quantum yield increases are an essential component of the Southern Ocean phytoplankton response to iron, P. Natl. Acad. Sci. USA, 105, 4775–4780, https://doi.org/10.1073/pnas.0705006105, 2008.

Holm-Hansen, O. and Riemann, B.: Chlorophyll *a* Determination: Improvements in Methodology, Oikos, 30, 3, 438–447, https://doi.org/10.2307/3543338, 1978.

Hughes, D. J., Campbell, D. A., Doblin, M. A., Kromkamp, J. C., Lawrenz, E., Moore, C. M., Oxborough, K., Prášil, O., Ralph, P. J., Alvarez, M. F., and Suggett, D. J.: Roadmaps and Detours: Active Chlorophyll-*a* Assessments of Primary Productivity Across Marine and Freshwater Systems, Environ. Sci. Technol., 52, 12039–12054, https://doi.org/10.1021/acs.est.8b03488, 2018.

Kauko, H. M., Moreau, S., and Hattermann, T.: Southern Ocean Ecosystem cruise 2019 vertical in situ chlorophyll a profiles, Norwegian Polar Institute [data set], https://doi.org/10.21334/npolar.2021.5e510f85, 2020.

Kauko, H. M., Hattermann, T., Ryan-Keogh, T., Singh, A., de Steur, L., Fransson, A., Chierici, M., Falkenhaug, T., Hallfredsson, E. H., Bratbak, G., and Tsagaraki, T.: Phenology and environmental control of phytoplankton blooms in the Kong Håkon VII Hav in the Southern Ocean, Front. Mar. Sci., 8, 623856, https://doi.org/10.3389/fmars.2021.623856, 2021.

Kauko, H. M., Moreau, S., Rózañska, M., and Wiktor, J. M.: Southern Ocean Ecosystem cruise 2019 phytoplankton taxonomy and abundance, Norwegian Polar Institute [data set], https://doi.org/10.21334/npolar.2022.283e500c, 2022a.

Kauko, H. M., Assmy, P., Peeken, I., Różańska-Pluta, M., Wiktor, J. M., Bratbak, G., Singh, A., Ryan-Keogh, T. J., and Moreau, S.: First phytoplankton community assessment of the Kong Håkon VII Hav, Southern Ocean, during austral autumn, Biogeosciences, 19, 5449–5482, https://doi.org/10.5194/bg-19-5449-2022, 2022b.

Khatiwala, S., Primeau, F., and Hall, T.: Reconstruction of the history of anthropogenic CO_2 concentrations in the ocean, Nature, 462, 346–349, https://doi.org/10.1038/nature08526, 2009.

Kirk, J. T. O.: Light and photosynthesis in aquatic ecosystems, Cambridge University Press, https://doi.org/10.1017/CBO9780511623370, 1994.

Klunder, M. B., Laan, P., Middag, R., De Baar, H. J. W., and van Ooijen, J. C.: Dissolved iron in the Southern Ocean (Atlantic sector), Deep-Sea Res. Pt. II, 58, 2678–2694, https://doi.org/10.1016/j.dsr2.2010.10.042, 2011.

Kolber, Z., Zehr, J., and Falkowski, P.: Effects of Growth Irradiance and Nitrogen Limitation on Photosynthetic Energy Conversion in Photosystem II. Plant Physiol., 88, 923–929, https://doi.org/10.1104/pp.88.3.923, 1988.

Kolber, Z. S., Barber, R. T., Coale, K. H., Fitzwateri, S. E., Greene, R. M., Johnson, K. S., Lindley, S., and Falkowski, P. G.: Iron limitation of phytoplankton photosynthesis in the equatorial Pacific Ocean, Nature, 371, 145–149, https://doi.org/10.1038/371145a0, 1994.

Kolber, Z. S., Prášil, O., and Falkowski, P. G.: Measurements of variable chlorophyll fluorescence using fast repetition rate techniques: defining methodology and experimental protocols, BBA-Bioenergetics, 1367, 88–106, https://doi.org/10.1016/S0005-2728(98)00135-2, 1998.

Lancelot, C., Mathot, S., Veth, C., and de Baar, H.: Factors controlling phytoplankton ice-edge blooms in the marginal ice-zone of the northwestern Weddell Sea during sea ice retreat 1988: field observations and mathematical modelling, Polar Biol., 13, 377–387, https://doi.org/10.1007/BF01681979, 1993.

Lannuzel, D., Schoemann, V., de Jong, J., Chou, L., Delille, B., Becquevort, S., and Tison, J. L.: Iron study during a time series in the western Weddell pack ice, Mar. Chem., 108, 85–95, https://doi.org/10.1016/j.marchem.2007.10.006, 2008.

Lannuzel, D., Vancoppenolle, M., van Der Merwe, P., De Jong, J., Meiners, K. M., Grotti, M., Nishioka, J., and Schoemann, V.: Iron in sea ice: Review and new insightsIron in sea ice: Review and new insights, Elementa, 4, 000130, https://doi.org/10.12952/journal.elementa.000130, 2016.

Lindsey, R. and Scott, M.: What are Phytoplankton?, https://earthobservatory.nasa.gov/features/Phytoplankton (last access: 20 July 2023), 2010.

Lis, H., Shaked, Y., Kranzler, C., Keren, N., and Morel, F. M.: Iron bioavailability to phytoplankton: an empirical approach, ISME J., 9, 1003–1013, https://doi.org/10.1038/ismej.2014.199, 2015.

Lucas, M., Seeyave, S., Sanders, R., Moore, C. M., Williamson, R., and Stinchcombe, M.: Nitrogen uptake responses to a naturally Fe-fertilised phytoplankton bloom during the 2004/2005 CROZEX study, Deep-Sea Res. Pt. II, 54, 2138–2173, https://doi.org/10.1016/j.dsr2.2007.06.017, 2007.

Lutjeharms, J. R. E., Walters, N. M., and Allanson, B. R.: Oceanic frontal systems and biological enhancement, in: Antarctic Nutrient Cycles and Food Webs, Springer Berlin Heidelberg, 11–21, https://doi.org/10.1007/978-3-642-82275-9_3, 1985.

Mahowald, N. M., Baker, A. R., Bergametti, G., Brooks, N., Duce, R. A., Jickells, T. D., Kubilay, N., Prospero, J. M., and Tegen, I.: Atmospheric global dust cycle and iron inputs to the ocean, Global Biogeochem. Cy., 19, GB4025, https://doi.org/10.1029/2004GB002402, 2005.

Martin, J. H. and Fitzwater, S. E.: Iron deficiency limits phytoplankton growth in the north-east Pacific subarctic, Nature, 331, 341–343, https://doi.org/10.1038/331341a0, 1988.

Martin, J. H., Gordon, R. M., and Fitzwater, S. E.: Iron in Antarctic waters. Nature, 345, 156–158, https://doi.org/10.1038/345156a0, 1990.

Martin, J. H., Gordon, M., and Fitzwater, S. E.: The case for iron, Limnol. Oceanogr., 36, 1793–1802, https://doi.org/10.4319/lo.1991.36.8.1793, 1991.

Millard, R. C., Owens, W. B., and Fofonoff, N. P.: On the calculation of the Brunt-Väisäla frequency, Deep-Sea Res. Pt. A, 37, 167–181, https://doi.org/10.1016/0198-0149(90)90035-T, 1990.

Milligan, A. J. and Harrison, P. J.: Effects of non-steady-state iron limitation on nitrogen assimilatory enzymes in the marine diatom thalassiosira weissflogii (BACILLARIOPHYCEAE), J. Phycol., 36, 78–86, https://doi.org/10.1046/j.1529-8817.2000.99013.x, 2000.

Mitchell, B. G., Brody, E. A., Holm-Hansen, O., McClain, C., and Bishop, J.: Light limitation of phytoplankton biomass and macronutrient utilization in the Southern Ocean, Limnol. Oceanogr., 36, 1662–1677, https://doi.org/10.4319/lo.1991.36.8.1662, 1991.

Moore, C. M., Hickman, A. E., Poulton, A. J., Seeyave, S., and Lucas, M. I.: Iron–light interactions during the CROZet natural iron bloom and EXport experiment (CROZEX): II – Taxonomic responses and elemental stoichiometry, Deep-Sea Res. Pt. II, 54, 2066–2084, https://doi.org/10.1016/j.dsr2.2007.06.015, 2007a.

Moore, C. M., Seeyave, S., Hickman, A. E., Allen, J. T., Lucas, M. I., Planquette, H., Pollard, R. T., and Poulton, A. J.: Iron-light interactions during the CROZet natural iron bloom and EXport experiment (CROZEX) I: Phytoplankton growth and photophysiology, Deep-Sea Res. Pt. II, 54, 2045–2065, https://doi.org/10.1016/j.dsr2.2007.06.011, 2007b.

Moore, C. M., Mills, M. M., Arrigo, K. R., Berman-Frank, I., Bopp, L., Boyd, P. W., Galbraith, E. D., Geider, R. J., Guieu, C., Jaccard, S. L., Jickells, T. D., La Roche, J., Lenton, T. M., Mahowald, N. M., Marañón, E., Marinov, I., Moore, J. K., Nakatsuka, T., Oschlies, A., Saito, M. A., Thingstad, T. F., Tsuda, A., and Ulloa, O.: Processes and patterns of oceanic nutrient limitation, Nat. Geosci., 6, 701–710, https://doi.org/10.1038/ngeo1765, 2013.

Moore, J. K. and Abbott, M. R.: Surface chlorophyll concentrations in relation to the Antarctic Polar Front: seasonal and spatial patterns from satellite observations, J. Marine Syst., 37, 69–86, https://doi.org/10.1016/S0924-7963(02)00196-3, 2002.

Moore, J. K., Doney, S. C., Glover, D. M., and Fung, I. Y.: Iron cycling and nutrient-limitation patterns in surface waters of the World Ocean, Deep-Sea Res. Pt. II, 49, 463–507, https://doi.org/10.1016/S0967-0645(01)00109-6, 2001.

Moreau, S., Boyd, P. W., and Strutton, P. G.: Remote assessment of the fate of phytoplankton in the Southern Ocean sea-ice zone, Nat. Commun., 11, 1–9, https://doi.org/10.1038/s41467-020-16931-0, 2020.

Moreau, S., Hattermann, T., de Steur, L., Kauko, H. M., Ahonen, H., Ardelan, M. V., Assmy, P., Chierici, M., Descamps, S., Dinter, T., Falkenhaug, T., Fransson, A., Grønningsæter, E., Hallfredsson, E. H., Huhn, O., Lebrun, A., Lowther, A., Lübcker, N., Monteiro, P. M. S., Peeken, I., Roychoudhury, A., Różańska, M., Ryan-Keogh, T. J., Sanchez, N., Singh, A., Simonsen, J.-H., Steiger, N., Thomalla, S. J., van Tonder, A., Wiktor, J. M., and Steen, H.: Wind-driven upwelling of iron sustains dense blooms and food webs in the eastern Weddell Gyre, Nat. Commun., 14, 1303, https://doi.org/10.1038/s41467-023-36992-1, 2023.

Mtshali, T. N., van Horsten, N. R., Thomalla, S. J., Ryan-Keogh, T. J., Nicholson, S. A., Roychoudhury, A. N., Bucciarelli, E., Sarthou, G., Tagliabue, A., and Monteiro, P. M. S.: Seasonal Depletion of the Dissolved Iron Reservoirs in the Sub-Antarctic Zone of the Southern Atlantic Ocean, Geophys. Res. Lett., 46, 4386–4395, https://doi.org/10.1029/2018GL081355, 2019.

National Geophysical Data Center/NESDIS/NOAA/U.S. Department of Commerce: ETOPO1, Global 1 Arc-minute Ocean Depth and Land Elevation from the US National Geophysical Data Center (NGDC), Research Data Archive at the National Center for Atmospheric Research, Computational and Information Systems Laboratory, https://doi.org/10.5065/D69Z92Z5, 2011.

Nicholson, S. A., Lévy, M., Jouanno, J., Capet, X., Swart, S., and Monteiro, P. M. S.: Iron Supply Pathways Between the Surface and Subsurface Waters of the Southern Ocean: From Winter Entrainment to Summer Storms, Geophys. Res. Lett., 46, 14567–14575, https://doi.org/10.1029/2019GL084657, 2019.

Pollard, R., Sanders, R., Lucas, M., and Statham, P.: The Crozet Natural Iron Bloom and Export Experiment (CROZEX), Deep-Sea Res. Pt. II, 54, 1905–1914, https://doi.org/10.1016/j.dsr2.2007.07.023, 2007.

Price, N. M., Ahner, B. A., and Morel, F. M.: The equatorial Pacific Ocean: Grazer-controlled phytoplankton populations in an iron-limited ecosystem 1, Limnol. Oceanogr., 39, 520–534, https://doi.org/10.4319/LO.1994.39.3.0520, 1994.

Racault, M. F., Sathyendranath, S., and Platt, T.: Impact of missing data on the estimation of ecological indicators from satellite ocean-colour time-series, Remote Sens. Environ., 152, 15–28, https://doi.org/10.1016/j.rse.2014.05.016, 2014.

Raven, J. A.: Predictions of Mn and Fe use efficiencies of phototrophic growth as a function of light availability for growth and of C assimilation pathway, New Phytol., 116, 1–18, https://doi.org/10.1111/j.1469-8137.1990.tb00505.x, 1990.

Raven, J. A., Evans, M. C. W., and Korb, R. E.: The role of trace metals in photosynthetic electron transport in O-2-evolving organisms, Photosynth. Res., 60, 111–149, https://doi.org/10.1023/a:1006282714942, 1999.

Richert, I., Yager, P. L., Dinasquet, J., Logares, R., Riemann, L., Wendeberg, A., Bertilsson, S., and Scofield, D. G.: Summer comes to the Southern Ocean: how phytoplankton shape bacterioplankton communities far into the deep dark sea, Ecosphere, 10, e02641, https://doi.org/10.1002/ecs2.2641, 2019.

Roháček, K.: Chlorophyll fluorescence parameters: The definitions, photosynthetic meaning, and mutual relationships, Photosynthetica, 40, 13–29, https://doi.org/10.1023/A:1020125719386, 2002.

Ryan-Keogh, T. J.: Understanding the role of chlorophyll fluorescence in nutrient stress, Doctoral dissertation, University of Southampton, http://eprints.soton.ac.uk/id/eprint/362003 (last access: 1 March 2022), 2014.

Ryan-Keogh, T. J. and Robinson, C.: Phytoplankton Photophysiology Utilities: A Python Toolbox for the Standardization of Processing Active Chlorophyll-*a* Fluorescence Data, Front. Mar. Sci. Aquat. Physiol., 8, 525414, https://doi.org/10.3389/fmars.2021.525414, 2021.

Ryan-Keogh, T. J., Macey, A. I., Nielsdóttir, M. C., Lucas, M. I., Steigenberger, S. S., Stinchcombe, M. C., Achterberg, E. P., Bibby, T. S., and Moore, C. M.: Spatial and temporal development of phytoplankton iron stress in relation to bloom dynamics in the high-latitude North Atlantic Ocean, Limnol. Oceanogr., 58, 533–545, https://doi.org/10.4319/lo.2013.58.2.0533, 2013.

Ryan-Keogh, T. J., DeLizo, L. M., Smith, W. O., Sedwick, P. N., McGillicuddy, D. J., Moore, C. M., and Bibby, T. S.: Temporal progression of photosynthetic-strategy in phytoplankton in the Ross Sea, Antarctica, J. Marine Syst., 166, 87–96, https://doi.org/10.1016/j.jmarsys.2016.08.014, 2017.

Ryan-Keogh, T. J., Thomalla, S. J., Mtshali, T. N., van Horsten, N. R., and Little, H. J.: Seasonal development of iron limitation in the sub-Antarctic zone, Biogeosciences, 15, 4647–4660, https://doi.org/10.5194/bg-15-4647-2018, 2018.

Ryan-Keogh, T. J., Thomalla, S. J., Monteiro, P. M., and Tagliabue, A.: Multidecadal trend of increasing iron stress in Southern Ocean phytoplankton, Science, 379, 834–840, https://doi.org/10.1126/science.abl5237, 2023.

Salgado-Hernanz, P. M., Racault, M. F., Font-Muñoz, J. S., and Basterretxea, G.: Trends in phytoplankton phenology in the Mediterranean Sea based on ocean-colour remote sensing, Remote Sens. Environ., 221, 50–64, https://doi.org/10.1016/j.rse.2018.10.036, 2019.

Samanta, S., Cloete, R., Loock, J., Rossouw, R., and Roychoudhury, A. N.: Determination of trace metal (Mn, Fe, Ni, Cu, Zn, Co, Cd and Pb) concentrations in seawater using single quadrupole ICP-MS: A comparison between offline and online preconcentration setups, Minerals 11, 1289, https://doi.org/10.3390/min11111289, 2021.

Sathyendranath, S., Brewin, R. J., Brockmann, C., Brotas, V., Calton, B., Chuprin, A., Cipollini, P., Couto, A. B., Dingle, J., Doerffer, R., and Donlon, C.: An ocean-colour time series for use in climate studies: the experience of the ocean-colour climate change initiative (OC-CCI), Sensors, 19, 4285, https://doi.org/10.3390/s19194285, 2019.

Schuback, N., Flecken, M., Maldonado, M. T., and Tortell, P. D.: Diurnal variation in the coupling of photosynthetic electron transport and carbon fixation in iron-limited phytoplankton in the NE subarctic Pacific, Biogeosciences, 13, 1019–1035, https://doi.org/10.5194/bg-13-1019-2016, 2016.

Schuback, N., Tortell, P. D., Berman-Frank, I., Campbell, D. A., Ciotti, A., Courtecuisse, E., Erickson, Z. K., Fujiki, T., Halsey, K., Hickman, A. E., and Huot, Y.: Single-turnover variable chlorophyll fluorescence as a tool for assessing phytoplankton photosynthesis and primary productivity: opportunities, caveats and recommendations, Front. Mar. Sci., 8, 690607, https://doi.org/10.3389/fmars.2021.690607, 2021.

Sedwick, P. N., DiTullio, G. R., Hutchins, D. A., Boyd, P. W., Griffiths, F. B., Crossley, A. C., Trull, T. W., and Quéguiner, B.: Limitation of algal growth by iron deficiency in the Australian Subantarctic region, Geophys. Res. Lett., 26, 2865–2868, https://doi.org/10.1029/1998GL002284, 1999.

Sedwick, P. N., Bowie, A. R., and Trull, T. W.: Dissolved iron in the Australian sector of the Southern Ocean (CLIVAR SR3 section): meridional and seasonal trends, Deep-Sea Res. Pt. I, 55, 911–925, https://doi.org/10.1016/j.dsr.2008.03.011, 2008.

Singh, A., Fietz, S., Thomalla, S. J., Sanchez, N., Ardelan, M. V., Moreau, S., Kauko, H. M., Fransson, A., Chierici, M., Samanta, S., Mtshali, T. N., Roychoudhury, A. N., and Ryan-Keogh, T. J.: Photophysiological response of autumn phytoplankton in the Antarctic Sea-Ice Zone, Zenodo [data set], https://doi.org/10.5281/zenodo.6322943, 2022.

Smith, W. O., Dinniman, M. S., Tozzi, S., DiTullio, G. R., Mangoni, O., Modigh, M., and Saggiomo, V.: Phytoplankton photosynthetic pigments in the Ross Sea: Patterns and relationships among functional groups, J. Marine Syst., 82, 177–185, https://doi.org/10.1016/j.jmarsys.2010.04.014, 2010.

Soppa, M. A., Völker, C., and Bracher, A.: Diatom phenology in the Southern Ocean: mean patterns, trends and the role of climate oscillations, Remote Sens., 8, 420, https://doi.org/10.3390/rs8050420, 2016.

Strzepek, R. F. and Harrison, P. J.: Photosynthetic architecture differs in coastal and oceanic diatoms, Nature, 431, 689–692, https://doi.org/10.1038/nature02954, 2004.

Strzepek, R. F., Maldonado, M. T., Hunter, K. A., Frew, R. D., and Boyd, P. W.: Adaptive strategies by Southern Ocean phytoplankton to lessen iron limitation: Uptake of organically complexed iron and reduced cellular iron requirements, Limnol. Oceanogr., 56, 1983–2002, https://doi.org/10.4319/lo.2011.56.6.1983, 2011.

Strzepek, R. F., Hunter, K. A., Frew, R. D., Harrison, P. J., and Boyd, P. W.: Iron-light interactions differ in Southern Ocean phytoplankton, Limnol. Oceanogr., 57, 1182–1200, https://doi.org/10.4319/lo.2012.57.4.1182, 2012.

Strzepek, R. F., Boyd, P. W., and Sunda, W. G.: Photosynthetic adaptation to low iron, light, and temperature in Southern Ocean phytoplankton, P. Natl. Acad. Sci. USA, 116, 4388–4393, https://doi.org/10.1073/pnas.1810886116, 2019.

Suggett, D., Kraay, G., Holligan, P., Davey, M., Aiken, J., and Geider, R.: Assessment of photosynthesis in a spring cyanobacterial bloom by use of a fast repetition rate fluorometer, Limnol. Oceanogr., 46, 802–810, https://doi.org/10.4319/lo.2001.46.4.0802, 2001.

Suggett, D. J., Moore, C. M., Hickman, A. E., and Geider, R. J.: Interpretation of fast repetition rate (FRR) fluorescence: Signatures of phytoplankton community structure versus physiological state, Mar. Ecol.-Prog. Ser., 376, 1–19, https://doi.org/10.3354/meps07830, 2009.

Sunda, W. G.: Trace metal interactions with marine phytoplankton, Biol. Oceanogr., 6, 411–442, 1989.

Sunda, W. G. and Huntsman, S. A.: Iron uptake and growth limitation in oceanic and coastal phytoplankton, Mar. Chem., 50, 189–206, https://doi.org/10.1016/0304-4203(95)00035-P, 1995.

Swart, S., Thomalla, S. J., and Monteiro, P. M. S.: The seasonal cycle of mixed layer dynamics and phytoplankton biomass in the Sub-Antarctic Zone: A high-resolution glider experiment, J. Marine Syst., 147, 103–115, https://doi.org/10.1016/j.jmarsys.2014.06.002, 2015.

Tagliabue, A., Sallée, J. B., Bowie, A. R., Lévy, M., Swart, S., and Boyd, P. W.: Surface-water iron supplies in the Southern Ocean sustained by deep winter mixing, Nat. Geosci., 7, 314–320, https://doi.org/10.1038/ngeo2101, 2014.

Tagliabue, A., Bowie, A. R., Boyd, P. W., Buck, K. N., Johnson, K. S., and Saito, M. A.: The integral role of iron in ocean biogeochemistry, Nature, 543, 51–59, https://doi.org/10.1038/nature21058, 2017.

Takahashi, T., Sutherland, S. C., Sweeney, C., Poisson, A., Metzl, N., Tilbrook, B., Bates, N., Wanninkhof, R., Feely, R. A., Sabine, C., Olafsson, J., and Yukihiro, N.: Global sea–air CO_2 flux based on climatological surface ocean pCO_2, and seasonal biological and temperature effects, Deep-Sea Res. Pt. II, 49, 1601–1622, https://doi.org/10.1016/S0967-0645(02)00003-6, 2002.

Takahashi, T., Sutherland, S. C., Wanninkhof, R., Sweeney, C., Feely, R. A., Chipman, D. W., Hales, B., Friederich, G., Chavez, F., Sabine, C., and Watson, A.: Climatological mean and decadal change in surface ocean pCO_2, and net sea–air CO_2 flux over the global oceans, Deep-Sea Res. Pt. II, 56, 554–577, https://doi.org/10.1016/j.dsr2.2008.12.009, 2009.

Taylor, M. H., Losch, M., and Bracher, A.: On the drivers of phytoplankton blooms in the Antarctic marginal ice zone: A modeling approach, J. Geophys. Res.-Ocean, 118, 63–75, https://doi.org/10.1029/2012JC008418, 2013.

Thomalla, S. J., Fauchereau, N., Swart, S., and Monteiro, P. M. S.: Regional scale characteristics of the seasonal cycle of chlorophyll in the Southern Ocean, Biogeosciences, 8, 2849–2866, https://doi.org/10.5194/bg-8-2849-2011, 2011.

Trimborn, S., Thoms, S., Bischof, K., and Beszteri, S.: Susceptibility of two Southern Ocean phytoplankton key species to iron limitation and high light, Front. Mar. Sci., 6, 167, https://doi.org/10.3389/fmars.2019.00167, 2019.

Van Oijen, T., Van Leeuwe, M. A., Granum, E., Weissing, F. J., Bellerby, R. G. J., Gieskes, W. W. C., and de Baar, H. J. W.: Light rather than iron controls photosynthate production and allocation in Southern Ocean phytoplankton populations during austral autumn, J. Plankton Res., 26, 885–900, https://doi.org/10.1093/plankt/fbh088, 2004.

Viljoen, J. J., Philibert, R., Van Horsten, N., Mtshali, T., Roychoudhury, A. N., Thomalla, S., and Fietz, S.: Phytoplankton response in growth, photophysiology and community structure to iron and light in the Polar Frontal Zone and Antarctic waters, Deep-Sea Res. Pt. I, 141, 118–129, https://doi.org/10.2495/EEIA100071, 2018.

Vink, S. and Measures, C. I.: The role of dust deposition in determining surface water distributions of Al and Fe in the South West Atlantic, Deep-Sea Res. Pt. II, 48, 2787–2809, https://doi.org/10.1016/S0967-0645(01)00018-2, 2001.

Wu, M., McCain, J. S. P., Rowland, E., Middag, R., Sandgren, M., Allen, A. E., and Bertrand, E. M.: Manganese and iron deficiency in Southern Ocean Phaeocystis antarctica populations revealed through taxon-specific protein indicators, Nat. Commun., 10, 3582, https://doi.org/10.1038/s41467-019-11426-z, 2019.

Yoon, J.-E., Yoo, K.-C., Macdonald, A. M., Yoon, H.-I., Park, K.-T., Yang, E. J., Kim, H.-C., Lee, J. I., Lee, M. K., Jung, J., Park, J., Lee, J., Kim, S., Kim, S.-S., Kim, K., and Kim, I.-N.: Reviews and syntheses: Ocean iron fertilization experiments – past, present, and future looking to a future Korean Iron Fertilization Experiment in the Southern Ocean (KIFES) project, Biogeosciences, 15, 5847–5889, https://doi.org/10.5194/bg-15-5847-2018, 2018.